The dual function monoclonal antibodies VIR-7831 and VIR-7832 demonstrate potent in vitro and in vivo activity against SARS-CoV-2

Andrea L. Cathcart[1], Colin Havenar-Daughton[1], Florian A. Lempp[1], Daphne Ma[1], Michael A. Schmid[2], Maria L. Agostini[1], Barbara Guarino[2], Julia Di iulio[1], Laura E. Rosen[1], Heather Tucker[1], Joshua Dillen[1], Sambhavi Subramanian[1], Barbara Sloan[1], Siro Bianchi[2], Dora Pinto[2], Christian Saliba[2], Jason A Wojcechowskyj[1], Julia Noack[1], Jiayi Zhou[1], Hannah Kaiser[1], Arthur Chase[1], Martin Montiel-Ruiz[1], Exequiel Dellota Jr.[1], Arnold Park[1], Roberto Spreafico[1], Anna Sahakyan[1], Elvin J. Lauron[1], Nadine Czudnochowski[1], Elisabetta Cameroni[1], Sarah Ledoux[1], Adam Werts[3], Christophe Colas[1], Leah Soriaga[1], Amalio Telenti[1], Lisa A. Purcell[1], Seungmin Hwang[1], Gyorgy Snell[1], Herbert W. Virgin[1], Davide Corti[2], Christy M. Hebner[1*]

[1]Vir Biotechnology, San Francisco, California 94158, USA

[2]Humabs Biomed SA, a subsidiary of Vir Biotechnology, 6500 Bellinzona, Switzerland

[3]Lovelace Biomedical, Albuquerque, New Mexico 87108, USA

*corresponding author: chebner@vir.bio

ABSTRACT

VIR-7831 and VIR-7832 are dual action monoclonal antibodies (mAbs) targeting the spike glycoprotein of severe acute respiratory syndrome coronavirus 2 (SARS-CoV-2). VIR-7831 and VIR-7832 were derived from a parent antibody (S309) isolated from memory B cells of a 2003 severe acute respiratory syndrome coronavirus (SARS-CoV) survivor. Both mAbs contain an "LS" mutation in the Fc region to prolong serum half-life and potentially enhance distribution to the respiratory mucosa. In addition, VIR-7832 encodes an Fc GAALIE mutation that has been shown previously to evoke CD8+ T-cells in the context of an in vivo viral respiratory infection. VIR-7831 and VIR-7832 potently neutralize wild-type and variant authentic virus in vitro as well as variant pseudotyped viruses. In addition, they retain activity against monoclonal antibody resistance mutations conferring reduced susceptibility to currently authorized mAbs. The VIR-7831/VIR-7832 epitope does not overlap with mutational sites in current variants of concern and continues to be highly conserved among circulating sequences consistent with the high barrier to resistance observed in vitro. Furthermore, both mAbs can recruit effector mechanisms in vitro that may contribute to clinical efficacy via elimination of infected host cells. In vitro studies with these mAbs demonstrated no enhancement of infection. In a Syrian Golden hamster proof-of concept wildtype SARS-CoV-2 infection model, animals treated with VIR-7831 had less weight loss, and significantly decreased total viral load and infectious virus levels in the lung compared to a control mAb. Taken together, these data indicate that VIR-7831 and VIR-7832 are promising new agents in the fight against COVID-19.

INTRODUCTION

The coronavirus disease (COVID-19) pandemic caused by severe acute respiratory syndrome coronavirus 2 (SARS-CoV-2) has resulted in more than 153 million confirmed cases and over 3.2 million deaths

48 worldwide[1]. SARS-CoV-2 infection results in a broad range of disease severity[2]. Infection fatality rates
49 increase significantly with age, with 28.3% of COVID-19 patients over the age of 85 succumbing to
50 disease[2]. However, even in mild-to-moderate COVID-19 patients, significant post-infection sequelae can
51 affect overall health and cause long-term disability[3]. While multiple SARS-CoV-2 vaccines are now
52 authorized for use, issues of supply, vaccine hesitancy and emergence of variants may prevent rapid
53 attainment of herd immunity[4–9]. In addition, there may be individuals who remain at risk despite
54 vaccination due to disease or underlying immunodeficiency. Thus, additional interventions and potential
55 prophylactic agents are needed to reduce morbidity and mortality due to COVID-19.

56 Several monoclonal antibodies (mAbs) targeting the SARS-CoV-2 spike protein have recently been
57 authorized for use in early treatment of COVID-19 patients[10–13] and clinical data have been reported to
58 show promising results in treatment and prophylactic studies[12–15]. However, rapidly spreading variants
59 including those from the United Kingdom (B.1.1.7), South Africa (B.1.351) and Brazil (P.1) exhibit
60 reduced susceptibility in vitro to currently authorized antibodies that target the receptor binding motif
61 (RBM) of the viral spike (S) glycoprotein [10,11,16,17]. Therefore, mAbs targeting unique S epitopes are
62 needed for use alone or in combination with current agents for the treatment and prevention of COVID-
63 19. Furthermore, in addition to viral neutralization, antibodies possessing potent effector function to aid in
64 the killing of virally infected cells and the elicitation of T cell immunity could significantly assist in
65 halting disease progression[18–20].

66 VIR-7831 and VIR-7832 are dual action mAbs derived from the parent antibody S309 identified from a
67 2003 SARS-CoV survivor[21]. These mAbs target an epitope containing a glycan (at position N343) that is
68 highly conserved within the Sarbecovirus subgenus in a region of the S receptor binding domain (RBD)
69 that does not compete with angiotensin converting enzyme 2 (ACE2) binding[22]. This epitope does not
70 overlap with mutations observed in current variants of concern[10,11,16,17]. The variable region of VIR-7831
71 and VIR-7832 have been engineered for enhanced developability. In addition, both antibodies possess an
72 Fc "LS" mutation that confers extended half-life by binding to the neonatal Fc receptor and potentially

enhances distribution to the respiratory mucosa [23–25]. VIR-7832 is identical to VIR-7831 with the exception of the addition of a 3 amino acid GAALIE (G236A, A330L, I332E) modification to the Fc domain[26]. The GAALIE modification has previously been shown in vitro to enhance binding to FcγIIa and FcγIIIa receptors, decrease affinity for FcγIIb compared to typical IgG1 and evoke protective CD8+ T-cells in the context of viral respiratory infection in vivo [27,28].

Here we characterize the antiviral potential of VIR-7831 and VIR-7832. These mAbs effectively neutralize SARS-CoV-2 live virus in vitro as well as in pseudotyped virus assays against emerging variants of concern and variants that confer resistance to currently authorized mAbs[29]. In addition to the neutralizing capacity, both antibodies demonstrate potent effector function and mediate antibody dependent cellular cytotoxicity (ADCC) and antibody dependent cellular phagocytosis (ADCP) in vitro. Furthermore, resistance selection experiments and epitope conservation analyses indicate the potential for a high barrier to resistance. Data derived from the Syrian golden hamster model demonstrates efficacy in a proof-of-concept in vivo model. Taken together, these data indicate that VIR-7831 and VIR-7832 are promising key components of the arsenal in the fight against COVID-19.

RESULTS

VIR-7831 and VIR-7832 bind SARS-CoV-2 spike and effectively neutralize live virus in vitro.

Previously published work showed that S309 bound SARS-CoV-2 recombinant and cell surface-associated S and neutralized live virus in vitro[21]. We initiated these studies by repeating and extending these earlier results. To determine the binding activity of VIR-7831 and VIR-7832 to the SARS-CoV-2 S, enzyme-linked immunosorbent assay (ELISA), surface plasmon resonance (SPR) and flow cytometry assays were utilized. VIR-7831 and VIR-7832 bound to recombinant S RBD (amino acids 331-541) with EC_{50} values of 20.40 ng/mL and 14.9 ng/mL, respectively, by ELISA (**Figure 1a**). Using SPR, both antibodies demonstrated potent binding to recombinant S RBD with an equilibrium constant (Kd) of 0.21 nM (**Figure 1b**). As antibody recognition of cell surface-bound S could mediate killing of virally infected cells, flow cytometry-based studies using cells transiently transfected with a S-encoding plasmid were

98 used to examine antibody binding to cell surface-expressed S trimer. By this method, both VIR-7831 and
99 VIR-7832 bound efficiently to surface-expressed S (**Figure 1c**).

100 To examine neutralization capacity, VIR-7831 and VIR-7832 were tested in a VeroE6 cell-based live
101 SARS-CoV-2 virus system against the Washington 2019 (wild-type) virus as well as against the UK
102 (B.1.1.7), South Africa (B.1.351) and Brazil (P.1) variants. Concentration-dependent viral neutralization
103 of the Washington 2019 strain was observed for both antibodies, with geometric mean $IC_{50/90}$ values of
104 100.1/186.3 ng/mL and 78.3/253.1 ng/mL, respectively (**Figure 1d**). $IC_{50/90}$ values observed for VIR-7831
105 and VIR-7832 against the South Africa and Brazil variant viruses were similar to those against the wild-
106 type strain. A slight shift in the VIR-7831/VIR-7832 $IC_{50/90}$ compared to wild-type was observed for the
107 UK variant. VIR-7831 showed a 3-fold and 4.1-fold shift in IC_{50} and IC_{90}, respectively, against the UK
108 variant compared to wild-type while VIR-7832 had a 3.1-fold shift in IC_{50} and 3.7-fold shift in IC_{90} versus
109 wild-type (**Figure 1d, Table 1)**. As variant evolution is a natural part of SARS-CoV-2 biology and
110 emerging live virus variants are not always readily accessible for testing, a vesicular stomatitis virus
111 (VSV)-based pseudotyped virus system targeting Vero E6 cells was used to examine VIR-7831 and VIR-
112 7832 neutralization against emergent variants (**Table 2**). Fold-changes in VIR-7831 and VIR-7832 IC_{50}
113 values compared to wild-type against pseudotyped virus expressing spike from the South Africa, UK or
114 Brazil variant were similar to those observed in the authentic virus system. VIR-7831 was tested against
115 an extended panel of pseudotyped viruses incorporating emerging variants from the Americas, Europe
116 and Africa. Fold-changes in VIR-7831 IC_{50} values against these variants ranged from 0.6- to 1.1-fold
117 indicating that VIR-7831 retains activity against these spike variants (**Table 2**).

118 **VIR-7831 and VIR-7831 exhibit potent effector function in vitro.** Although direct antiviral
119 mechanisms are crucial to provide protection, Fc-dependent mechanisms mediated by interaction with Fc
120 gamma receptors (FcγRs) on immune cells or with complement, can contribute to overall potency in vivo.
121 The potential for VIR-7831 and VIR-7832 to mediate effector functions were assessed in vitro by

122 measuring binding to FcγRs and C1q and in assays designed to demonstrate antibody-dependent cellular
123 cytotoxicity (ADCC) or antibody-dependent cellular phagocytosis (ADCP)[31–34].

124 Antibody binding to the human activating FcγRIIa (low-affinity R131 and high affinity H131 alleles),
125 FcγRIIIa (low-affinity F158 and high-affinity V158 alleles), and to the inhibitory FcγRIIb were examined
126 using SPR (**Supplemental figure 1a**). VIR-7831 similarly bound both the H131 and R131 alleles of
127 FcγRIIa and binds FcγRIIb. VIR-7831 bound both FcγRIIIa alleles, with reduced binding to the F158
128 allele compared to V158, as is characteristic for human IgG1[35]. Binding of VIR-7831 to C1q was similar
129 to the parental antibody (S309-LS) (**Supplemental figure 1b**). As previously reported for antibodies
130 encoding the GAALIE mutation[26,36], VIR-7832 bound with comparatively higher affinity to activating
131 FcγRIIa and FcγRIIIa than VIR-7831 (**Supplemental figure 1a**). Conversely, VIR-7832 showed reduced
132 affinity for FcγIIb and abrogation of binding to C1q (**Supplemental figure 1b**).

133 The antibodies were also assessed for the ability to activate human FcγRIIa, FcγRIIb or FcγRIIIa, using a
134 Jurkat cell reporter assay[37] (**Figure 2a-d**). S309-GRLR, which contains the effector function-abrogating
135 G236R, L328R mutations was used as a negative control. Cells stably transfected with the SARS-CoV-2
136 spike protein (CHO-CoV-2-Spike) served as target cells. Both VIR-7831 and the parental S309-LS
137 activated signaling of the higher-affinity allele FcγRIIa (H131) but did so less efficiently than the
138 GAALIE-containing antibody VIR-7832 (**Figure 1a**) while VIR-7831, VIR-7832 and S309-LS induced
139 similar low-level activation of the inhibitory receptor FcγRIIb (**Figure 1b**). VIR-7831 demonstrated
140 substantially lower activation of FcγRIIIa F158 versus V158 as expected while VIR-7832 showed
141 increased activation of both alleles of FcγRIIIa (F158 and V158) (**Figures c,d**).

142 To further elucidate the effector function potential of the antibodies, ADCC and ADCP assays were
143 performed using donor PBMCs or NK cells as effector cells and CHO cells stably expressing S (CHO-
144 CoV-2-Spike) as target cells (**Figure 2e-g**). The ability of antibodies to activate NK cell-mediated killing
145 was measured in vitro using two genotyped donors expressing homozygous low-affinity (F/F158) or high-
146 affinity (V/V158) (**Figure 2e-f**). Compared to the parental mAb S309-LS, VIR-7831 had slightly

147 increased capacity to induce NK cell-mediated ADCC when using cells from either F/F158 or V/V158
148 donors. As expected, VIR-7832 induced NK cell-mediated ADCC in cells from donors expressing the
149 low-affinity F/F158 allele of FcγIIIa more efficiently than VIR-7831. These results were confirmed with
150 NK cells from a heterozygous donor (F/V 158).

151 The ability of VIR-7831 and VIR-7832 to facilitate ADCP by primary $CD14^+$ monocytes was measured in
152 vitro by exposing freshly isolated human PBMCs to CHO-CoV-2-Spike cells that were pre-incubated
153 with antibody (**Figure 2g**). VIR-7831, VIR-7832 and S309-LS induced similar levels of ADCP by $CD14^+$
154 monocytes. These results indicate that VIR-7831 and VIR-7832 have the potential to trigger ADCC and
155 ADCP of cells displaying SARS CoV-2 S protein.

156 **Subneutralizing levels of VIR-7831 and VIR-7832 do not enhance virus uptake, replication or**
157 **cytokine production in vitro.** One potential concern with any antibody therapeutic targeting a viral agent
158 is the possibility of antibody-dependent enhancement (ADE). ADE is an in vivo phenomenon in which
159 the presence of an antibody worsens disease. There are several in vitro assays that may provide plausible
160 correlates for ADE in vivo, though none of these have been proven relevant to COVID-19 as to date ADE
161 has not been observed in trials of monoclonal antibodies or plasma[13,15,38,39]. ADE can occur by several
162 potential mechanisms[40]. Poorly neutralizing antibodies or subneutralizing levels of antibody could
163 theoretically facilitate enhanced virus entry and infection through Fc receptor interactions. A second
164 theoretical mechanism involves antibody-antigen complex formation leading to enhanced cytokine
165 production. A third mechanism of ADE has been observed in a porcine model of influenza where the
166 kinetics of viral fusion to the target cell was enhanced in a Fab-dependent manner by fusion-enhancing
167 non-neutralizing antibodies[41,42].

168 To explore whether VIR-7831 and VIR-7832 exhibit in vitro activities that might be related to ADE in
169 vivo, we evaluated SARS-CoV-2 replication in human cells that express FcγRs: monocyte-derived
170 dendritic cells (moDCs), peripheral blood mononuclear cells (PBMCs) and the human U937 macrophage
171 cell line (**Supplemental Figure 2a-b**). Subneutralizing concentrations of VIR-7831 and VIR-7832 were

172 precomplexed with SARS-CoV-2 (MOI =0.01) and added to target cells. Using immunostaining methods,
173 at 24 hours post-infection no productive entry of SARS-CoV-2 into moDCs, PBMCs, or U937 cells was
174 observed in the presence or absence of either mAb, while VeroE6 control cells demonstrated
175 internalization in all conditions evaluated. Reduced internalization of SARS-CoV-2 in VeroE6 cells was
176 observed at the highest concentration of VIR-7831 and VIR-7832 (p-value <0.05), indicating effective
177 virus neutralization prevented virus entry. Using a focus forming assay, virus replication and secretion of
178 infectious virus were detectable by 48 hours post-infection in VeroE6 cells, with comparable levels of
179 replication in the presence or absence of VIR-7831 or VIR-7832. However, no replication of SARS-CoV-
180 2 was detected in moDCs, PBMCs or U937 cells regardless of antibody treatment, indicating lack of
181 productive SARS-CoV-2 infection of these cells, consistent with previously published data[43].

182 To evaluate the potential for VIR-7831 and VIR-7832 to enhance cytokine release upon SARS-CoV-2
183 infection in FcγR-expressing cells, cytokines and chemokines were measured in the supernatants from
184 cells infected with SARS-CoV-2-in the presence of VIR-7831 or VIR-7832 (**Supplemental figure 2c**).
185 Levels of IFN-γ, IL-10, IL-6, IL 8, IP-10, MCP-1, and TNF-α in the supernatant were quantified by MSD
186 at 24- and 48-hours post-infection. For all cell types evaluated, cytokine/chemokine production was
187 similar between all antibody concentrations tested and the no antibody control at both 24- and 48-hours
188 post-infection. Taken together, these in vitro data indicate that neither VIR-7831 nor VIR-7832 exhibit in
189 vitro activities that have been proposed to possibly correlate with ADE in vivo.

190 **VIR-7831 and VIR-7832 have a high barrier to resistance in vitro and do not display cross-**
191 **resistance with other SARS-CoV-2 mAbs.** We next determined whether resistant variants could be
192 elicited by serial passage of SARS-CoV-2 in the presence of VIR-7832. As VIR-7831 and VIR-7832
193 differ only in the Fc region of the antibody, resistance selection experiments were conducted with VIR-
194 7832 as a proxy for both antibodies. SARS-CoV-2 was subjected to 10 passages in the presence of VIR-
195 7832 at fixed concentrations of ~10x, 20x, 50x or 100x IC_{50} (1, 2, 5, or 10 μg/mL) in VeroE6 cells. No
196 CPE was detected in wells passaged with antibody through 10 passages, while CPE was observed in the

197 no antibody control in all passages. Similarly, no virus was detected by focus forming assay at any
198 concentration of VIR-7832 through all 10 passages even at the lowest concentration tested.

199 As no viral breakthrough was observed in the fixed concentration resistance selection, a second method
200 was employed wherein SARS-CoV-2 virus was passaged in sub-IC_{50} concentrations of antibody followed
201 by subsequent passaging in the presence of increasing concentrations of mAb in an attempt to force
202 resistance emergence (**Supplemental Figure 3**). Passaging was performed in duplicate wells to account
203 for founder effects, and concentration increases for each well were based on CPE observations. Five
204 sequential passages were conducted using increasing concentrations of VIR-7832 at 0.5, 1, 2, 5 and ~10x
205 IC_{50} (0.05, 0.1, 0.2, 0.5, 1 µg/mL; **Supplemental Figure 3a**), though no CPE was observed by passages 4
206 and 5 (0.5 and 1 µg/mL, respectively) indicating that variants originally selected at the lower
207 concentrations were either unfit or susceptible to the higher concentrations of antibody. To further assess
208 whether resistance mutations could be generated, selection was restarted using passage 3 virus generated
209 with ~2x IC_{50} (0.2 µg/mL) of VIR-7832 in duplicate wells at ~2x and ~5x IC_{50} (0.2, 0.5 µg/mL),
210 generating two passage lineages (**Supplemental Figure 3b-c**).

211 Supernatants were evaluated for detectable virus at each passage by focus forming assay and cell
212 supernatants from viral passages containing detectable virus were tested in SARS-CoV-2 neutralization
213 assays to evaluate IC_{50} shifts as a marker of reduced susceptibility (**Supplemental Table 1**). With the
214 exception of passage 8, modest fold changes were observed, with shifts in IC_{50} values ranging from 5.4-
215 to 6.5-fold compared to the wild-type SARS-CoV-2 stock virus. In lineage 1, the passage 8 virus
216 displayed a >10-fold shift in IC_{50} (greater than highest concentration tested). Sequence analysis detected
217 an identical 4 amino acid insertion in the N-terminal domain (215-216insKLRS) and 5 amino acid
218 deletion in correspondence of the furin cleavage site (675-679del) in both lineages at all passages
219 sequenced, as well as the amino acid substitution E340A in lineage 1, and R682W, and V1128F in
220 lineage 2. The deletion at amino acids 675-679 has been previously described during passaging of SARS-
221 CoV-2 in tissue culture suggesting enrichment to be a result of cell culture adaptation[44] while the 215-

222 216insKLRS was detected in the input virus. Neither 215-216insKLRS nor R682W variants were highly
223 enriched with passaging (**Supplemental Table 1**) and enrichment of 675-679del and V1128F did not
224 profoundly alter the VIR-7832 IC_{50}. However, appearance of the E340A variant at 98.7% did correlate
225 with a >10-fold shift in IC_{50} suggesting this variant may confer resistance.

226 To evaluate whether amino acid variants identified in the resistance selection conferred reduced
227 susceptibility to VIR-7831 and VIR-7832, neutralization of pseudotyped viruses encoding the S variants
228 was assessed (**Supplemental Table 2**). VIR-7831 and VIR-7832 neutralized R682W and V1128F SARS-
229 CoV-2 pseudotyped virus spike variants with IC_{50} values similar to wild type (< 2-fold change in IC_{50})
230 indicating that these variants do not alter susceptibility. In contrast, E340A conferred reduced
231 susceptibility to VIR-7831 and VIR-7832 (> 100-fold change in IC_{50}) indicating that E340A is a VIR-
232 7831/VIR-7832 monoclonal antibody resistance mutation (MARM).

233 As VIR-7831/VIR-7832 demonstrated a unique in vitro resistance profile, we investigated the potential
234 for cross-resistance to MARMs that confer reduced susceptibility to the authorized monoclonal antibodies
235 bamlanivimab, imdevimab and casirivimab [10,11,45–47] using pseudotyped virus. Notably, some of these
236 mutations are found in highly prevalent variants of concern[17,30,48]. VIR-7831 effectively neutralized
237 pseudotyped viruses expressing spike MARMs that alter bamlanivimab, casirivimab and/or imdevimab
238 activity (**Table 3**). Fold changes in IC_{50} values compared to wild-type were <3-fold for 18/19 variants
239 tested. A modest 3.4-fold shift in the VIR-7831 IC_{50} was observed for the V445A variant that confers
240 reduced susceptibility to imdevimab. These data indicate that VIR-7831/VIR-7832 does not display cross-
241 resistance with currently authorized mAbs and supports the potential combination use of VIR-7831/VIR-
242 7832 with other mAb therapeutics.

243 **The VIR-7831/VIR-7832 epitope is highly conserved among SARS-CoV-2 sequences.** The parental
244 antibody of VIR-7831 and VIR-7832 (S309) binds to a highly conserved sarbecovirus epitope that is
245 potentially intolerant of variation. To investigate the current state of epitope conservation, >1,000,000
246 spike sequences from SARS-CoV-2 deposited in the GISAID database as of April 16, 2021 were

247 examined for epitope variation. More than 99.9% conservation is seen for those amino acids comprising
248 the epitope among currently available sequences for all positions including 17/23 amino acid positions
249 that were ≥99.99 conserved (**Table 4**).

250 VIR-7831 activity against viral mutants carrying single substitutions in the epitope was assessed in
251 pseudotyped virus assays. VIR-7831 effectively neutralized epitope variants at most amino acid positions
252 tested (**Table 5**). Variants at two positions, E340 and P337, resulted in significant IC_{50} shifts indicating
253 reduced susceptibility to VIR-7831. Moderate shifts in potency were observed for P337H and P337T
254 variants (7.50- and 5.38-fold, respective) while more significant shifts in potency were observed for
255 P337L/R and E340A/K/G (27-fold to >276-fold). Notably, these variants are detected in a low number of
256 sequences and do not have a pattern that suggest emergence in the GISAID database (45 and 63 variant
257 counts out of >1,000,000 sequences for P337 and E340, respectively). This observation is consistent with
258 the possibility that variations at these positions come with a fitness cost to the virus.

259 **VIR-7831 reduces weight loss, total viral load and infectious virus levels in a hamster model of**
260 **SARS-CoV-2 infection.** To evaluate the efficacy of VIR-7831 in vivo, the hamster model was utilized.
261 As it was unknown what effect the LS mutation would have in the hamster, a non-LS version of VIR-
262 7831 (SGHmAb-no-LS) was used for these experiments. Hamsters were administered SGHmAb-no-LS
263 intraperitoneally at Day -1 (30, 5, 0.5 or 0.05 mg/kg) or Day -2 (15, 5, 0.5 or 0.05 mg/kg) prior to
264 intranasal SARS-CoV-2 inoculation (**Figure 3a**). Using body weight as a marker of degree of clinical
265 disease, doses of ≥5mg/kg resulted in significantly reduced weight loss at Day 4 compared to controls.
266 (**Figure 3b-e**). Significant decreases in lung viral load were also observed at ≥5mg/kg as measured by
267 RT-qPCR (**Figures f-g**). Day 4 $TCID_{50}$ measurements indicated that antibody administered at ≥0.5 mg/kg
268 resulted in significantly lower levels of infectious virus in lung tissue compared to controls (**Figure 3h-i**).
269 Notably, across these experiments, no enhancement of disease was observed in animals receiving
270 SGHmAb-no-LS based on changes in weight, viral RNA in the lungs, or $TCID_{50}$ infectious virus levels.

271 Collectively, these data indicate that VIR-7831 prevented in a dose-dependent fashion virus replication
272 and morbidity in SARS-CoV-2 challenged hamsters without signs of ADE at any dose tested.

273 **DISCUSSION**

274 Here we show the in vitro and in vivo preclinical characterization of VIR-7831 and VIR-7832, two
275 monoclonal antibodies being advanced into clinical studies[49–51]. Both antibodies demonstrate high-affinity
276 binding to S in vitro, including on the surface of cells, and effectively neutralize wildtype SARS-CoV-2
277 in a live virus assay. VIR-7831 and VIR-7832 retain activity against the UK B.1.1.7, South Africa
278 B.1.351 and Brazil P.1 variants in an authentic virus system, consistent with data using pseudotyped
279 viruses. VIR-7831 bind C1q, activate FcγRs and demonstrate ADCC and ADCP in vitro. Experiments in
280 the hamster model of SARS-CoV-2 infection show proof-of-concept efficacy in vivo. Notably, in vitro
281 and in vivo data did not provide any supporting evidence that these antibodies would demonstrate ADE in
282 a clinical setting.

283 That VIR-7831 and VIR-7832 retain activity against spike variants in authentic virus and pseudotyped
284 virus assays is a key finding at this stage of the pandemic. With the increased transmissibility and
285 potential for more severe disease observed with these viruses, the availability of therapeutic or
286 prophylactic mAbs that remains active against these variants is essential. Current in vitro data indicate
287 that the E484K variant found in both B.1.351, P.1 and other emerging independent lineages, and also
288 recently found in combination with B.1.1.7[52], confers reduced susceptibility to multiple currently
289 authorized monoclonal antibodies possibly lessening the utility of these antibodies or, worse, rendering
290 them ineffective. In addition to retaining activity against key variants of concern, in pseudotyped virus
291 experiments VIR-7831 showed no significant cross-resistance with variants that reduce the activity of
292 authorized mAbs. These data additionally demonstrate the uniqueness of VIR-7831 and VIR-7832 and
293 further highlight the utility VIR-7831 and VIR-7832 could have, alone or in combination, as clinical
294 agents.

295 Notably, even over a year into the pandemic, the VIR-7831/VIR-7832 epitope remains highly conserved
296 among available sequences of circulating virus with ≥99.9% conservation of epitope amino acids. This is
297 consistent with the value of the strategy used for isolation of monoclonal antibodies that neutralize both
298 SARS-CoV and SARS-CoV-2 based on the idea that these two virulent human viruses are
299 phylogenetically divergent within the sarbecovirus subgenus. Furthermore, MARMs identified at
300 positions P337 and E340 are present at very low levels among current sequences. That amino acids P337
301 and E340 remain ≥99.99% conserved at this stage of the pandemic indicates that variants at these
302 positions may confer disadvantageous effects on the virus, consistent with the conservation of this epitope
303 across the sarbecovirus family[21].

304 Viral variants of concern for RBM-targeting mAbs are quickly spreading[53]. The vaccines presently being
305 deployed around the world generate high-titer neutralizing antibodies that target the S protein RBM.
306 Importantly, the RBM is highly immunodominant for responses to natural infection[54]. Vaccine-induced
307 and convalescent immunity may therefore potentially put further mutational pressure on the RBM
308 sequence to evade such antibody responses. In contrast, antibody responses overlapping with the VIR-
309 7831/VIR-7832 epitope are limited after infection [54], possibly because of the shielding effect of the highly
310 conserved N343 glycan. In this regard the epitope may face less vaccine- or infection-generated immune
311 pressure, potentially preserving this conserved epitope long-term.

312 Recent data have indicated that the cells used to generate live virus stocks and overexpression of
313 ACE2/TMPRSS2 in target cells used for assays can affect mAb activity in vitro[29,55]. The VIR-7831/VIR-
314 7832 parental antibody S309 seems particularly sensitive to in vitro methods using ACE2 overexpressing
315 cells[55]. It is therefore notable that VIR-7831 displays significant efficacy in an in vivo proof-of-concept
316 SARS-CoV-2 infection experiment using hamsters despite the fact that patterns of engagement of hamster
317 FcRs by human IgG1 antibodies may not reflect patterns of human IgG1 antibodies with their cognate
318 human FcRs. These findings argue that in vitro data derived from such ACE2 and/or TMPRSS2
319 overexpression cell lines do not accurately reflect the in vivo antiviral capacity of tested mAbs.

320 Furthermore, that the significant in vivo effects of VIR-7831 in the hamster model likely occurred in the
321 absence of full effector functions due to species-specific interactions between antibodies and FcRs, argues
322 that effects in COVID-19 patients incorporating both the neutralization capacity of the antibody plus the
323 ability to harness the strength of the immune system could lead to positive clinical outcomes.

324 The clinical potential of VIR-7832, with the inclusion of the GAALIE Fc mutation, is of special interest
325 in the context of SARS-CoV-2 infection. Previously published data by the Ravetch laboratory comparing
326 the in vivo efficacy of a hemagglutinin-targeting mAb with and without inclusion of the GAALIE
327 mutation in a transgenic humanized FcγR mouse model of influenza infection demonstrated superior
328 efficacy of the GAALIE-containing antibody in both therapeutic and prophylactic experiments[26]. These
329 effects were mediated by protective $CD8^+$ T cell responses elicited by the GAALIE antibody. Clinical
330 data examining the contribution of the adaptive immune response in SARS-CoV-2 infection indicate that
331 poor T cell induction correlates with severe disease (reviewed in [56]). Thus, the potential for VIR-7832 to
332 augment the T cell response to SARS-CoV-2 infection could conceivably play a crucial role in limiting
333 progression to severe COVID-19 disease or in treatment of severe established disease. This latter
334 possibility is supported by recent publications showing that monoclonal antibodies with effector functions
335 are especially effective in the therapeutic setting via recruitment of tissue-protective monocyte functions
336 [19], and that potency of antibodies in the pre-clinical mouse model does not correlate with in vitro
337 neutralizing activity of antibodies[18].

338 Taken together, these data indicate that VIR-7831 and VIR-7832 could play a powerful role in the fight
339 against COVID-19 through the dual action of broadly neutralizing activity paired with engagement of the
340 immune system through effector function capabilities.

341

342 **METHODS**

343 **Cells.** Vero E6 cells (ATCC) and Lenti-X 293T cells (Takara) were cultured in Dulbecco's Modified
344 Eagle's medium (DMEM), 10% FBS, 1x Penicillin-Streptomycin at 37°C, 5% CO_2.

345 **Monoclonal Antibodies.** VIR-7831 and VIR-7832 were produced at WuXi Biologics (China). SGHmAb-
346 no-LS, S309-LS, and S309-GRLR were produced at Humabs Biomed SA, a subsidiary of Vir
347 Biotechnology (Bellinzona, Switzerland) in expiCHO cells transiently co-transfected with plasmids
348 expressing the heavy and light chain, as previously described [57].

349 **Virus. S**ARS-CoV-2 isolates USA-WA1/2020, UK/VUI/3/2020, hCoV-19/South Africa/KRISP-
350 K005325/2020 and hCoV-19/Japan/TY7-503/2021 were obtained from BEI Resources. To propagate
351 SARS-CoV-2, VeroE6 or VeroE6-TMPRSS2 cells were seeded at $10X10^6$ cells in T175 flasks in growth
352 media and infected the next day at a MOI of 0.001 in virus propagation media. Virus was adsorbed for 1
353 hour at 37°C. Virus inoculum was removed, flasks were washed once with PBS, 25 mL of infection
354 media was added to the cells and flasks were incubated at 37°C. Supernatants were collected at 48 hours
355 post-infection once cytopathic effect was visible, centrifuged at 500 x g for 5 minutes, followed by a
356 second centrifugation at 1000 x g for 5 minutes. Clarified supernatants were then aliquoted and stored at -
357 80°C. Virus titers were determined using a plaque assay on VeroE6 cells, using standard methods.
358 Briefly, 10-fold dilutions of virus stock were incubated in 6 well plates with 2.4% colloidal cellulose
359 overlay for 24 hours. Cells were fixed with 4% PFA for 30 minutes at room temperature (RT),
360 permeabilized with 0.125% Triton X-100, stained with anti-SARS-CoV-2 nucleocapsid antibody at
361 1:5000 and goat anti-rabbit IgG HRP at 1:5000. Plaque forming units (PFU) were visualized with
362 TrueBlue reagent.

363 **In vitro binding ELISA.** For the ELISA assay, 96-well plates were coated with 100 µl/well recombinant
364 SARS-CoV2 RBD diluted in assay diluent (1% BSA/PBS) at a final concentration of 2 µg/mL and
365 incubated overnight at 4°C. Plates were washed three times with 300 µl/well wash buffer using an
366 automated washer. Assay diluent (100 µl/well) was added to block the plates and incubated for 1 hour at
367 room temperature (RT) with shaking. Assay diluent was removed, and plates washed three times with

368 wash buffer. Serial 1:3 dilutions of mAb (concentration range from 6 µg/mL to 0.33 ng/mL) in assay
369 diluent were dispensed at 100 µl/well and incubated 1 hour at RT with shaking, then washed three times
370 with wash buffer. The HRP-conjugated secondary antibody reagent (1:5,000 dilution in assay diluent)
371 was added to each well (100 µl/well) and incubated for 1 hour at RT with shaking. After three washes
372 with wash buffer, 100 µl/well of 2-component TMB peroxidase substrate solution was dispensed in each
373 well and developed for 5 minutes at RT. The reaction was stopped with 100 µL/well 1M H_2SO_4 and the
374 OD was read immediately at 450 nm on a SpectraMax M5 Microplate reader. EC_{50} values were calculated
375 using non-linear regression of log (agonist) versus response in Graph Pad Prism.

376 **Spike binding affinity quantification by SPR.** Antibody was diluted to 2 µg/mL (1 mL) in HBS-EP+
377 buffer and injected at 10 µL/min for 30 seconds across one flow cell of a CM5 sensor chip immobilized
378 with anti-human Fc antibody docked in a Biacore T200. SARS-CoV2-RBD diluted in HBS-EP+ buffer
379 was then injected at a single concentration, 1:3 dilutions from 100 nM to 3.7 nM, across both the flow cell
380 containing captured the antibody as well as a reference flow cell containing only anti-human Fc antibody.
381 Binding was measured with a flow rate of 30 µL/min and an injection time of 600 seconds; dissociation
382 was monitored for 1800 seconds after injection. Data were collected at 10 Hz. After each binding
383 measurement, regeneration reagent was injected to prepare the surface for a new cycle. Experiments were
384 performed at 25°C, with the samples held at 15 °C in the instrument prior to injection.

385 **Measurement of Binding to Human Fcγ Receptors by SPR.** Binding of VIR-7831 and VIR-7832 to
386 human recombinant FcγRs was measured by surface plasmon resonance (SPR) on a Biacore T200.
387 Briefly, Biotin CAPture Reagent (modified streptavidin) was injected across all flow cells of a CAP
388 sensor chip docked in a Biacore T200. Biotinylated Fc receptors at 1 µg/mL were injected across a single
389 flow cell at 10 µL/min for 60 seconds (one receptor per flow cell), with one flow cell reserved as a
390 reference surface. VIR 7831 or VIR-7832 at 100 µg/mL (diluted in HBS-EP+) were injected across all
391 flow cells for 200 seconds using a flow rate of 30 µL/min and association was monitored. Dissociation
392 was monitored for another 200 seconds after injection. Data was collected at 10 Hz. After each binding

393 measurement, CAP Regeneration reagent was injected to prepare the surface for a new cycle.
394 Experiments were performed at 25°C, with the samples held at 15°C in the instrument prior to injection.

395 **Measurement of Binding to Human Complement Protein C1q.** Binding of VIR-7831 and VIR-7832 to
396 human complement was measured by biolayer interferometry (BLI) using an Octet Red96 instrument
397 (FortéBio). Briefly, anti-human Fab (CH1-specific) sensors were used to capture VIR-7831 and VIR-
398 7832 at 10 µg/ml for 10 minutes. The IgG-loaded sensors were then exposed to kinetics buffer containing
399 3 µg/ml of purified human C1q for 4 minutes, followed by a dissociation step in the same buffer for
400 additional 4 minutes. Association and dissociation profiles were measured in real time as changes in the
401 interference pattern.

402 **Binding to Cell Surface Expressed SARS-CoV-2 Spike Protein.** The SARS-CoV-2 spike protein
403 coding sequence (YP_009724390.1, Wuhan-Hu-1 strain) was cloned into a cell expression plasmid under
404 the control of the human CMV promoter (phCMV1) to generate phCMV1 WT spike. ExpiCHO-S cells
405 were seeded the day before transfection at 3 x 10^6 cells/mL in ExpiCHO Expression Medium.
406 Immediately before transfection, the cells were seeded at 6 x 10^6 cells cells/mL in a volume of 15 mL in
407 125 mL shake flasks. Six µg of phCMV1 WT spike plasmid or vector control were diluted in 1.2 mL of
408 iced OptiPRO SFM., followed by addition of 48 µL of ExpiFectamine CHO Reagent and complexing for
409 1 minute at RT. The transfection mixture was added dropwise to cells with gentle swirling. Cells were
410 then incubated at 37°C, 8% CO2 with shaking for 42 hours. At 42 hours post-transfection, ExpiCHO-S
411 cells were harvested, washed twice with FACS buffer and resuspended at a concentration of 1.0 x 10^6
412 cell/mL in PBS. Cells (5 x 10^4 cells in 50 µl/wells) were dispensed into a 96-well V-bottom plate.
413 Antibody was serially diluted (1:4, 10 points) starting at a concentration of 10 µg/mL. Cells were pelleted
414 at 300 x g for 5 minutes and resuspended in 50 µL/well of antibody serial dilutions and plates were
415 incubated for 45 mins on ice. Cells were washed twice in FACS buffer. Alexa Fluor 647-labelled Goat
416 Anti-Human IgG secondary Ab was diluted 1:750 in FACS buffer and 50 µL was added to the cell pellet

417 for 15 min on ice. Cells were washed twice with FACS buffer, resuspended in 1% PFA. Data was
418 acquired by flow cytometry (CytoFlex LX).

419 **Pseudotyped virus production.** Lenti-X™ 293T cells were seeded in 10-cm dishes for 80% next day
420 confluency. The next day, cells were transfected with the plasmid pcDNA3.1(+)-spike-D19 (encoding the
421 SARS-CoV-2 spike protein) or pcDNA3.1(+)-spike-D19 variants using the transfection reagent TransIT-
422 Lenti according to the manufacturer's instructions. One day post-transfection, cells were infected with
423 VSV-luc (rVSVΔG; Kerafast) at an MOI of 3. The cell supernatant containing SARS-CoV-2 pseudotyped
424 virus was collected at day 2 post-transfection, centrifuged at 1000 x g for 5 minutes to remove cellular
425 debris, aliquoted and frozen at -80°C.

426 **In Vitro Neutralization of SARS-CoV-2 Pseudotyped Virus.** VeroE6 cells were seeded into flat
427 bottom tissue culture 96-well plates at 20,000 cells/well and cultured overnight at 37°C. Twenty-four
428 hours later, 9-point 1:4 serial dilutions of VIR-7831 were prepared in infection medium and each dilution
429 was tested in triplicate per plate (range: 20,000 to 0.3 ng/mL final concentration). SARS-CoV-2 virus
430 stock was diluted in infection media for a final concentration of 2000 plaque forming units per well (MOI
431 0.1). Antibody dilutions were added to virus and incubated for 30 minutes at 37°C. Media was removed
432 from the VeroE6 cells, mAb-virus complexes were added, and cells were incubated at 37°C. At 6 hours
433 post-infection, cells were fixed with 250 µL 4% PFA, incubated for 30 minutes at RT, then washed 3
434 times with PBS to remove residual PFA. The cells were permeabilized with 50 µL of 0.125% Triton X-
435 100 in PBS for 30 minutes at RT. The blocking buffer was removed, 50 µL of SARS-CoV-2 nucleocapsid
436 antibody at 1:2,000 in blocking buffer was added, and plate was incubated for 1 hour at RT. Plates were
437 washed three times with PBS and then incubated for 1 hour at RT with 50 µL/well of goat anti-rabbit-
438 Alexa647 secondary antibody at a final dilution of 1:1,000 mixed with 2 ug/mL Hoechst dye in blocking
439 buffer. After washing 5 times with PBS, 100 µL of fresh PBS was added for imaging. Plates were imaged
440 on a Cytation5 plate reader. Whole well images were acquired (12 images at 4X magnification per well)
441 and nucleocapsid-positive cells were counted using the manufacturer's software.

442 **Live virus neutralization.** VeroE6 cells were seeded into flat bottom tissue culture 96-well plates at
443 20,000 cells/well and cultured overnight at 37°C. Twenty-four hours later, 9-point 1:4 serial dilutions of
444 VIR-7831 were prepared in infection medium and each dilution was tested in triplicate per plate (range:
445 20,000 to 0.3 ng/mL final concentration). SARS-CoV-2 virus stock was diluted in infection media for a
446 final concentration of 2000 plaque forming units per well (MOI 0.1). Antibody dilutions were added to
447 virus and incubated for 30 minutes at 37°C. Media was removed from the VeroE6 cells, mAb-virus
448 complexes were added, and cells were incubated at 37°C. At 6 hours post-infection, cells were fixed with
449 250 µL 4% PFA, incubated for 30 minutes at RT, then washed 3 times with PBS to remove residual PFA.
450 The cells were permeabilized with 50 µL of 0.125% Triton X-100 in PBS for 30 minutes at RT. The
451 blocking buffer was removed, 50 µL of SARS-CoV-2 nucleocapsid antibody at 1:2,000 in blocking buffer
452 was added, and plate was incubated for 1 hour at RT. Plates were washed three times with PBS and then
453 incubated for 1 hour at RT with 50 µL/well of goat anti-rabbit-Alexa647 secondary antibody at a final
454 dilution of 1:1,000 mixed with 2 ug/mL Hoechst dye in blocking buffer. After washing 5 times with PBS,
455 100 µL of fresh PBS was added for imaging. Plates were imaged on a Cytation5 plate reader. Whole well
456 images were acquired (12 images at 4X magnification per well) and nucleocapsid-positive cells were
457 counted using the manufacturer's software..

458 **Determination of Viral Titer by Focus-Forming Assay.** One day prior to infection, $1.2X10^4$ VeroE6
459 cells were plated in black-walled, clear bottomed 96-well plates. Virus samples were diluted 1:5 in
460 infection media and adsorbed onto VeroE6 cells for one hour at 37°C. The cells were washed once and
461 overlaid with 1% methylcellulose/serum-containing media. At 24 hours post-infection, the
462 methylcellulose overlay was removed, and cells were washed with PBS. Cells were fixed with 4% PFA,
463 incubated for 30 minutes at RT, then washed with PBS to remove residual PFA. The cells were
464 permeabilized with 50 µL of 0.25% Triton X-100 in PBS for 30 minutes at RT. The Triton X-100 was
465 removed, cells were washed twice with PBS, and incubated with 50 µL of SARS-CoV-2 nucleocapsid
466 antibody at 1:2,000 in blocking buffer for one hour at RT. Plates were washed three times with PBS and

467 then incubated for one hour at RT with 50 µL/well of goat anti-rabbit-Alexa647 secondary antibody at
468 1:1,000 in blocking buffer. After washing three times with PBS, 50 µL of Hoechst dye at 1:1,000 in PBS
469 was added for imaging. Plates were imaged on a Cytation5 plate reader. Whole well images were
470 acquired (12 images at 4X magnification per well) and nucleocapsid-positive foci were counted using the
471 manufacturer's software and used to determine focus-forming units/mL supernatant (FFU/mL).

472 **Determination of mAb-Dependent Activation of Human FcγRIIa, FcγRIIIa or FcγRIIb.** VIR-7831,
473 VIR-7832, S309-LS, and a control mAb with abrogated FcγR binding, S309-GRLR, were serially diluted
474 6-fold in assay buffer from 10,000 ng/ml to 0.006 ng/ml. Nine-point serial dilutions of mAbs were
475 incubated with 12,500 (for FcγRIIIa and FcγRIIb) or 10,000 (for FcγRIIa) CHO-CoV-2-Spike cells per
476 96-plate well in a white, flat-bottom plate for 15 minutes at room temperature. Jurkat effector cells
477 expressing indicated FcγRs and stably transfected with an NFAT-driven luciferase gene were thawed,
478 diluted in assay buffer, and added to the plate at an effector to target cell ratio of 6:1 for FcRγIIIa and
479 FcγRIIb or 5:1 for FcγIIa. Control wells were also included that were used to measure antibody-
480 independent activation (containing target cells and effector cells but no antibody) and background
481 luminescence of the plate (wells containing assay buffer only). Plates were incubated for 18 hours at 37°C
482 with 5% CO2. Activation of human FcγRs in this bioassay results in the NFAT-mediated expression of
483 the luciferase reporter gene. Luminescence was measured with a luminometer after adding the Bio
484 GloTM Luciferase Assay Reagent according to the manufacturer's instructions. To control for
485 background, the mean of the relative luminescence units (RLU) values in wells containing only Assay
486 Buffer was calculated and subtracted from all data points. Data were expressed as the average of RLUs
487 over the background

488 **Determination of NK-Cell Mediated Antibody-Dependent Cellular Cytotoxicity.** Primary NK cell
489 activation was tested using freshly isolated cells from two previously genotyped donors expressing
490 homozygous low affinity (F158) or high affinity (V158) FcγRIIIa. Serial dilutions of mAbs (serially
491 diluted 10-fold in AIM-V Medium from 40,000 ng/ml to 0.075 ng/ml) were incubated with 7,500 CHO-

492 CoV-2 Spike cells per well of a 96 well round-bottom plate for 10 minutes. Target cell and antibody
493 mixtures were then incubated with primary human NK cells as effectors at an effector-to-target ratio of
494 10:1. ADCC was measured using lactate dehydrogenase (LDH) release as a readout according to the
495 manufacturer's instructions (Cytotoxicity Detection Kit (LDH), Roche) after 4 hours of incubation at
496 37°C. In brief, plates were centrifuged for 4 minutes at 400 x g, and 35 µl of supernatant was transferred
497 to a flat 384 well plate. LDH reagent was prepared and 35 µl were added to each well. Using a kinetic
498 protocol, the absorbance at 490 nm and 650 nm was measured once every 2 minutes for 8 minutes, and
499 the slope of the kinetics curve was used as result. The percent specific lysis was determined by applying
500 the following formula: (specific release – spontaneous release) / (maximum release - spontaneous release)
501 x 100.

502 **Determination of Monocyte-Mediated Antibody-Dependent Cellular Phagocytosis.** ADCP assays
503 were performed using human PBMCs freshly isolated from whole blood. CHO CoV-2-Spike cells were
504 used as target cells and were fluorescently labeled with PKH67 Fluorescent Cell Linker Kit (Sigma
505 Aldrich) prior to incubation with mAbs, according to manufacturer's instructions. Serial dilutions of
506 mAbs (serially diluted 5-fold from 5,000 ng/ml to 0.32 ng/ml in RPMI-1640 + L-glutamine supplemented
507 with 10% Hyclone FBS + 2x anti-anti (antibiotic-antimycotic)) were incubated with 10,000 CHO-CoV-2-
508 Spike cells per well of a 96 well polypropylene plate for 10 minutes. Primary PBMCs were fluorescently
509 labeled with Cell Trace Violet according to the manufacturer's instructions. Target cell and antibody
510 mixtures were then incubated with labeled PBMCs at an effector-to-target ratio of 16:1. After an
511 overnight incubation at 37°C, monocytes were stained with anti-human CD14-APC antibody (BD
512 Pharmingen). Antibody-mediated phagocytosis was determined by flow cytometry, gating on CD14+
513 cells that were double positive for cell trace violet and PKH67. Raw data were exported from the flow
514 cytometer into the flow cytometry analysis software FlowJo v10 (Becton Dickinson) for gating and
515 determination of the percentage of $CD14^+$ cells that were also double positive for cell trace violet and
516 PKH67. Cells expressing only cell trace violet or only PKH67 were used to set the positive staining gates.

517 **In vitro resistance selection.** The selection of variants in the presence of increasing concentrations of
518 VIR-7832 was conducted in VeroE6 cells. The day before infection, 6 x 10^4 VeroE6 cells were seeded in
519 24 well plates and incubated overnight at 37°C. The next day, 600 focus forming units (FFU) of SARS-
520 CoV-2 virus (MOI = 0.01) was incubated with 0.5X IC_{50} of VIR-7832 (0.05 µg/mL) at 37°C for one hour
521 in infection media. The mAb-virus complexes were adsorbed on VeroE6 cells for one hour at 37°C in
522 duplicate wells. After adsorption, cells were washed with DMEM and overlaid with infection media
523 containing 0.05 µg/mL VIR-7832. Control wells infected without antibody were included with each
524 passage. Infected cells were monitored visually for CPE daily. In general, when infected cells exhibited ≥
525 50% CPE, the culture supernatants were harvested, diluted 1:200, and added to fresh VeroE6 cells in 24-
526 well plates with equivalent or increasing concentrations of VIR-7832. At each passage, supernatant was
527 aliquoted and frozen at -80°C for titer and neutralization analyses.

528 **In vitro assessment of potential for ADE.** VeroE6 cells were plated at 1.25X10^4 cells/well one day prior
529 to infection. For each independent experiment, moDCs and PBMCs from five unique moDC donors and
530 six unique PBMC donors were used, with three unique donors used for each independent experiment.
531 Cryopreserved monocytes from unique donors were differentiated into moDCs for six days using human
532 moDC differentiation media according to the manufacturer's protocol. Cryopreserved PBMCs from
533 unique donors are thawed in the presence 0.3 mg/mL DNase and cultured in media for one day prior to
534 infection. On the day of infection, moDCs, PBMCs, and U937 cells were counted and plated at 7.5X10^4
535 cells/well.

536 To examine viral entry, 24 hours post-infection, cells were fixed with 4% PFA, incubated for 30 minutes
537 at RT, then washed with PBS to remove residual PFA. The cells were permeabilized with 50 µL of 0.25%
538 Triton X-100 in PBS for 30 minutes at RT. The Triton X-100 was removed, cells were washed twice with
539 PBS, and incubated with 50 µL of SARS-CoV-2 nucleocapsid antibody at 1:2,000 in blocking buffer for
540 one hour at RT. Plates were washed three times with PBS and then incubated for one hour at RT with 50
541 µL/well of goat anti-rabbit-Alexa647 secondary antibody at 1:1,000 in blocking buffer. After washing

542 three times with PBS, 50 µL of Hoechst dye at 1:1,000 in PBS was added for imaging. Plates were
543 imaged on a Cytation5 plate reader. Whole well images were acquired (12 images at 4X magnification
544 per well) and nucleocapsid-positive cells were counted using the manufacturer's software. The percent of
545 nucleocapsid+ cells was quantified using the Gen5 Imager software (Biotek, Vermont) as number of
546 Cy5+ cells, [(nucleocapsid+ cells)/number of Hoechst+ cells (total cells)]x100. Data was analyzed using
547 Prism v8.00 (GraphPad Software, La Jolla California USA, www.graphpad.com).

548 In order to quantify chemokines and cytokines from supernatants in a BSL2 laboratory, supernatants were
549 inactivated by 10 minutes exposure to UVC light at 5,000 µJ/cm2. Supernatants were diluted 1:5 in
550 infection media and levels of cytokines/chemokines were quantified using the U-plex 96-well assay
551 according to the manufacturer's protocol (Meso Scale Diagnostics, Rockville, MD). Quantification of
552 cytokines and chemokines were determined based on an 8-point standard curve in duplicate, provided by
553 the manufacturer. Cytokine data was analyzed using the Discovery Workbench v4.0.13 software (Meso
554 Scale Diagnostics). Data was graphed and statistical analyses were conducted using Prism software.

555 **Sequencing of SARS-CoV-2 Spike Gene.** To isolate nucleic acid from the supernatant of viral passages,
556 120 µL of cell supernatant was added to 360 µL of Trizol and stored at -80°C for further analysis. Trizol
557 collected samples from viral passages where a shift in neutralization > 2-fold relative to wild type was
558 detected were subjected to RNA isolation using PureLink RNA Mini Kit with the incorporation of on-
559 column PureLink DNase Treatment, following manufacturer's instructions. Reverse transcription
560 reactions were performed with 6 µL of purified RNA and oligoT primers using the NEB ProtoScript II
561 First Strand cDNA Synthesis kit, according to manufacturer's instructions. The resulting cDNA was used
562 as a template for PCR amplification of the spike gene using the KapaBiosystems polymerase (KAPA HiFi
563 HotStart ReadyMix) with primers 5' aattatcttggcaaaccacg-3' and 5' tgaggcttgtatcggtatcg-3'.
564 Amplification conditions included an initial 3 minutes at 95°C, followed by 28 cycles with 20 seconds at
565 98°C, 15 seconds at 62°C and 72°C for 2 minutes, with a final 4 minutes at 72°C. PCR products were
566 purified using AMPure XP beads following manufacturer's instructions. The size of the amplicon was

567 confirmed by analyzing 2 μL of PCR products using the Agilent D5000 ScreenTape System. Products
568 were quantified by analyzing 1 μL with the Quant-iT dsDNA High-Sensitivity Assay Kit. Twenty ng of
569 purified PCR product was used as input for library construction using the NEBNext Ultra II FS DNA
570 Library Prep kit following manufacturer's instructions. DNA fragmentation was performed for 13
571 minutes. NEBNext Multiplex Oligos for Illumina Dual Index Primer Set 1 was used for library
572 construction, with a total of 6 PCR cycles. Libraries size was determined using the Agilent D1000
573 ScreenTape System and quantified with the Quant iT dsDNA High-Sensitivity Assay Kit. Equal amounts
574 of each library were pooled together for multiplexing and 'Protocol A: Standard Normalization Method'
575 of the Illumina library preparation guide was used to prepare 8 pM final multiplexed libraries with 1%
576 PhiX spike-in for sequencing. The MiSeq Reagent Kit v3 (600-cycle) was used for sequencing the
577 libraries on the Illumina MiSeq platform, with 300 cycles for Read 1, 300 cycles for Read 2, 8 cycles for
578 Index 1, and 8 cycles for Index 2.

579 **Bioinformatics Analysis of Conservation.** Available genome sequences for SARS-CoV-2 were
580 downloaded from Global Initiative on Sharing All Influenza Data (GISAID; https://www.gisaid.org/) on
581 April 16, 2021. Bat and pangolin sequences were removed to yield human-only sequences. The spike
582 open reading frame was localized by aligning the reference protein sequence (NCBI reference sequence:
583 YP_009724390.1) to the genomic sequence of isolates with Exonerate v.2.4.0. Coding nucleotide
584 sequences were translated in silico using seqkit v.0.12.0. Multiple sequence alignment was performed
585 using MAFFT v.7.455. Variants were determined by comparison of aligned sequences to the reference
586 sequence using the R v3.6.3/Bioconductor v.3.10 package Biostrings v.2.54.0.

587 **In vivo studies.** Syrian golden hamster studies were conducted at Lovelace Biomedical (Albuquerque,
588 NM). Twelve- to sixteen-week-old male hamsters were interperitoneally administered a non-LS version
589 of VIR-7831 (SGHmAb-no-LS), control antibody or diluent Day -1 or Day -2 prior to virus challenge.
590 Animals were inoculated intranasally at Day 0 with 7.4×10^4 $TCID_{50}$ with SARS-CoV-2 (isolate USA-
591 WA1/2020). Animals were also weighed once daily in the morning beginning on study Day -10 and

592 continuing until the end of the study. Following euthanasia, RT-qPCR was performed on lung
593 homogenates using quantitative real-time PCR methods targeting the SARS-CoV-2 N gene and the
594 median tissue culture infections dose ($TCID_{50}$) was determined per Lovelace internal methodology.

595 **Author Contributions**

596 Conceived studies: A.L.C, C.H-D., F.A.P, D.M., M.S., L.S., A.T., L.A.P., S.H., G.S., H.W.V., D.C., C.M.H.
597 Designed studies and experiments: A.L.C, C.H.D., F.A.P, D.M., M.S., M.L.A., E. D., B.G., J.D., L.R.,A.C., A.S.,
598 R.S., J.W., N.C., E.C., S.L., C.C., D.P., C.S., J.N., A.P., A.W., L.S., A.T., L.A.P., S.H., G.S., H.W.V., D.C., C.M.H.
599 Performed experiments: D.M., M.S., M.L.A., B.G., J.D., E.D., A.S., L.R., H.T., J.D., S.S., D.P., C.S., J.N., B.S.,
600 S.B., J.W., J.Z., H.K., A.C., M.M-R., A.P., A.W., N.C., E.C. Analyzed and interpreted data: A.L.C., C.H-D., F.A.L.,
601 D.M., M.S., M.L.A., B.G., J.D., D.P., C.S., J.N., E.L., A.S., R.S., L.R., H.T., B.S., S.B., J.W., J.Z., H.K., A.C., M. M-
602 R., N.C., E.C., S.L., A.W., C.C., L.S., A.T., S.H., G.S., H.W.G, D.C., C.M.H. Prepared the manuscript with input
603 from all authors: A.L.C., G.S., A.T., L.P., D.C., H.W.G., C.M.H.

604 **Competing interests**

605 Some authors are current or former employees of Vir Biotechnology or Humabs BioMed SA (a fully-
606 owned subsidiary of Vir Biotechnology) and may hold shares in Vir Biotechnology. H.W.V. is a founder of
607 PierianDx and Casma Therapeutics.

608

609 **REFERENCES**

610

611 1. WHO Coronavirus Disease (COVID-19) Dashboard | WHO Coronavirus Disease (COVID-19)
612 Dashboard. https://covid19.who.int/.

613 2. Levin, A. T. *et al.* Assessing the age specificity of infection fatality rates for COVID-19:
614 systematic review, meta-analysis, and public policy implications. *Eur J Epidemiol* **35**, 1123–
615 1138 (2020).

616 3. Dennis, A. *et al.* Multi-organ impairment in low-risk individuals with long COVID.
617 doi:10.1101/2020.10.14.20212555.

618 4. Murphy, J. *et al.* Psychological characteristics associated with COVID-19 vaccine hesitancy
619 and resistance in Ireland and the United Kingdom. *Nat Commun* **12**, 29 (2021).

620 5. Khubchandani, J. *et al.* COVID-19 Vaccination Hesitancy in the United States: A Rapid
621 National Assessment. *J Commun Health* 1–8 (2021) doi:10.1007/s10900-020-00958-x.

622 6. Sallam, M. *et al.* High Rates of COVID-19 Vaccine Hesitancy and Its Association with
623 Conspiracy Beliefs: A Study in Jordan and Kuwait among Other Arab Countries. *Nato Adv Sci*
624 *Inst Se* **9**, 42 (2021).

625 7. Tegally, H. *et al.* Emergence and rapid spread of a new severe acute respiratory syndrome-
626 related coronavirus 2 (SARS-CoV-2) lineage with multiple spike mutations in South Africa.
627 *medRxiv* (2020) doi:10.1101/2020.12.21.20248640.

628 8. Naveca, F. *et al.* Phylogenetic relationship of SARS-CoV-2 sequences from Amazonas with
629 emerging Brazilian variants harboring mutations E484K and N501Y in the Spike protein -
630 SARS-CoV-2 coronavirus / nCoV-2019 Genomic Epidemiology - Virological.
631 https://virological.org/t/phylogenetic-relationship-of-sars-cov-2-sequences-from-amazonas-with-
632 emerging-brazilian-variants-harboring-mutations-e484k-and-n501y-in-the-spike-protein/585
633 (2011).

634 9. Rambaut, A. *et al.* Preliminary genomic characterisation of an emergent SARS-CoV-2 lineage
635 in the UK defined by a novel set of spike mutations - SARS-CoV-2 coronavirus / nCoV-2019
636 Genomic Epidemiology - Virological. https://virological.org/t/preliminary-genomic-
637 characterisation-of-an-emergent-sars-cov-2-lineage-in-the-uk-defined-by-a-novel-set-of-spike-
638 mutations/563 (2020).

639 10. Bamlanivimab EUA Letter of Authorization Reissue 02092021.
640 https://www.fda.gov/media/143603/download.

641 11. Casirivimab and Imdevimab EUA Fact Sheet for Healthcare Providers.
642 https://www.fda.gov/media/143892/download.

643 12. Lilly's neutralizing antibody bamlanivimab (LY-CoV555) prevented COVID-19 at nursing
644 homes in the BLAZE-2 trial, reducing risk by up to 80 percent for residents.
645 https://investor.lilly.com/node/44291/pdf.

646 13. Gottlieb, R. L. *et al.* Effect of Bamlanivimab as Monotherapy or in Combination With
647 Etesevimab on Viral Load in Patients With Mild to Moderate COVID-19. *Jama* **325**, 632–644
648 (2021).

649 14. Chen, P. *et al.* SARS-CoV-2 Neutralizing Antibody LY-CoV555 in Outpatients with Covid-
650 19. *New Engl J Med* (2020) doi:10.1056/nejmoa2029849.

651 15. Weinreich, D. M. *et al.* REGN-COV2, a Neutralizing Antibody Cocktail, in Outpatients with
652 Covid-19. *New Engl J Med* **384**, 238–251 (2020).

653 16. Starr, T. N. *et al.* Prospective mapping of viral mutations that escape antibodies used to treat
654 COVID-19. *Science* **371**, 850–854 (2021).

655 17. Wang, P. *et al.* Increased Resistance of SARS-CoV-2 Variants B.1.351 and B.1.1.7 to
656 Antibody Neutralization. *Biorxiv* 2021.01.25.428137 (2021) doi:10.1101/2021.01.25.428137.

657 18. Schäfer, A. *et al.* Antibody potency, effector function, and combinations in protection and
658 therapy for SARS-CoV-2 infection in vivo. *J Exp Med* **218**, (2020).

659 19. Winkler, E. S. *et al.* Human neutralizing antibodies against SARS-CoV-2 require intact Fc
660 effector functions and monocytes for optimal therapeutic protection. *Biorxiv* 2020.12.28.424554
661 (2020) doi:10.1101/2020.12.28.424554.

662 20. Bournazos, S. & Ravetch, J. V. Fcγ Receptor Function and the Design of Vaccination
663 Strategies. *Immunity* **47**, 224–233 (2017).

664 21. Pinto, D. *et al.* Cross-neutralization of SARS-CoV-2 by a human monoclonal SARS-CoV
665 antibody. *Nature* **583**, 290–295 (2020).

666 22. Pinto, D. *et al.* Cross-neutralization of SARS-CoV-2 by a human monoclonal SARS-CoV
667 antibody. *Nature* **583**, 290–295 (2020).

668 23. Ko, S.-Y. *et al.* Enhanced neonatal Fc receptor function improves protection against primate
669 SHIV infection. *Nature* **514**, 642 (2014).

670 24. Zalevsky, J. *et al.* Enhanced antibody half-life improves in vivo activity. *Nat Biotechnol* **28**,
671 157 (2010).

672 25. Gaudinski, M. R. *et al.* Safety and pharmacokinetics of the Fc-modified HIV-1 human
673 monoclonal antibody VRC01LS: A Phase 1 open-label clinical trial in healthy adults. *Plos Med*
674 **15**, e1002493 (2018).

675 26. Bournazos, S., Corti, D., Virgin, H. W. & Ravetch, J. V. Fc-optimized antibodies elicit CD8
676 immunity to viral respiratory infection. *Nature* 1–9 (2020) doi:10.1038/s41586-020-2838-z.

677 27. Weitzenfeld, P., Bournazos, S. & Ravetch, J. V. Antibodies targeting sialyl Lewis A mediate
678 tumor clearance through distinct effector pathways. *J Clin Invest* **129**, 3952–3962 (2019).

679 28. Bournazos, S., Corti, D., Virgin, H. W. & Ravetch, J. V. Fc-optimized antibodies elicit CD8
680 immunity to viral respiratory infection. *Nature* 1–9 (2020) doi:10.1038/s41586-020-2838-z.

681 29. Diamond, M. *et al.* SARS-CoV-2 variants show resistance to neutralization by many
682 monoclonal and serum-derived polyclonal antibodies. *Res Square* (2021) doi:10.21203/rs.3.rs-
683 228079/v1.

684 30. Chen, R. E. *et al.* Resistance of SARS-CoV-2 variants to neutralization by monoclonal and
685 serum-derived polyclonal antibodies. *Nat Med* 1–10 (2021) doi:10.1038/s41591-021-01294-w.

686 31. Kallewaard, N. L. *et al.* Structure and Function Analysis of an Antibody Recognizing All
687 Influenza A Subtypes. *Cell* **166**, 596–608 (2016).

688 32. DiLillo, D. J., Tan, G. S., Palese, P. & Ravetch, J. V. Broadly neutralizing hemagglutinin
689 stalk–specific antibodies require FcγR interactions for protection against influenza virus in vivo.
690 *Nat Med* **20**, 143–151 (2014).

691 33. Dunand, C. J. H. *et al.* Both Neutralizing and Non-Neutralizing Human H7N9 Influenza
692 Vaccine-Induced Monoclonal Antibodies Confer Protection. *Cell Host Microbe* **19**, 800–813
693 (2016).

694 34. Leon, P. E. *et al.* Optimal activation of Fc-mediated effector functions by influenza virus
695 hemagglutinin antibodies requires two points of contact. *Proc National Acad Sci* **113**, E5944–
696 E5951 (2016).

697 35. Bruhns, P. *et al.* Specificity and affinity of human Fcγ receptors and their polymorphic
698 variants for human IgG subclasses. *Blood* **113**, 3716–3725 (2009).

699 36. Weitzenfeld, P., Bournazos, S. & Ravetch, J. V. Antibodies targeting sialyl Lewis A mediate
700 tumor clearance through distinct effector pathways. *J Clin Invest* **129**, 3952–3962 (2019).

701 37. Cheng, Z. J. *et al.* Development of a robust reporter-based ADCC assay with frozen, thaw-
702 and-use cells to measure Fc effector function of therapeutic antibodies. *J Immunol Methods* **414**,
703 69–81 (2014).

704 38. Arvin, A. M. *et al.* A perspective on potential antibody-dependent enhancement of SARS-
705 CoV-2. *Nature* 1–11 (2020) doi:10.1038/s41586-020-2538-8.

706 39. Joyner, M. J. & Wright, R. S. Safety Update: CO VID-19 Convalescent Plasma in
707 20,000 Hospitalized Patients. *Mayo Clinic Proceedings* (2020).

40. Arvin, A. M. *et al.* A perspective on potential antibody-dependent enhancement of SARS-CoV-2. *Nature* **584**, 353–363 (2020).

41. Khurana, S. *et al.* Vaccine-induced anti-HA2 antibodies promote virus fusion and enhance influenza virus respiratory disease. *Sci Transl Med* **5**, 200ra114 (2013).

42. Winarski, K. L. *et al.* Antibody-dependent enhancement of influenza disease promoted by increase in hemagglutinin stem flexibility and virus fusion kinetics. *Proc National Acad Sci* **116**, 15194–15199 (2019).

43. Hui, K. P. Y. *et al.* Tropism, replication competence, and innate immune responses of the coronavirus SARS-CoV-2 in human respiratory tract and conjunctiva: an analysis in ex-vivo and in-vitro cultures. *Lancet Respir Medicine* (2020) doi:10.1016/s2213-2600(20)30193-4.

44. Liu, Z. *et al.* Identification of Common Deletions in the Spike Protein of Severe Acute Respiratory Syndrome Coronavirus 2. *J Virol* **94**, (2020).

45. Baum, A. *et al.* Antibody cocktail to SARS-CoV-2 spike protein prevents rapid mutational escape seen with individual antibodies. *Science* **369**, 1014–1018 (2020).

46. Thomson, E. C. *et al.* Circulating SARS-CoV-2 spike N439K variants maintain fitness while evading antibody-mediated immunity. *Cell* (2021) doi:10.1016/j.cell.2021.01.037.

47. Starr, T. N., Greaney, A. J., Dingens, A. S. & Bloom, J. D. Complete map of SARS-CoV-2 RBD mutations that escape the monoclonal antibody LY-CoV555 and its cocktail with LY-CoV016. doi:10.1101/2021.02.17.431683.

48. Wise, J. Covid-19: The E484K mutation and the risks it poses. *Bmj* **372**, n359 (2021).

49. VIR-7831 for the Early Treatment of COVID-19 in Outpatients - Full Text View - ClinicalTrials.gov. https://clinicaltrials.gov/ct2/show/NCT04545060?term=VIR-7831&draw=2&rank=2.

50. A Study of Immune System Proteins in Participants With Mild to Moderate COVID-19 Illness - Full Text View - ClinicalTrials.gov. https://clinicaltrials.gov/ct2/show/NCT04634409?term=VIR-7831&draw=2&rank=3.

51. Vir Biotechnology and GSK announce NHS-supported AGILE study to evaluate VIR-7832 in the early treatment of COVID-19 | GSK. *undefined* https://www.gsk.com/en-gb/media/press-releases/vir-biotechnology-and-gsk-announce-nhs-supported-agile-study-to-evaluate-vir-7832-in-the-early-treatment-of-covid-19/.

52. Wise, J. Covid-19: New coronavirus variant is identified in UK. *Bmj* **371**, m4857 (2020).

53. CoVariants. https://covariants.org/.

740 54. Piccoli, L. *et al.* Mapping neutralizing and immunodominant sites on the SARS-CoV-2 spike
741 receptor-binding domain by structure-guided high-resolution serology. *Cell* (2020)
742 doi:10.1016/j.cell.2020.09.037.

743 55. Rappazzo, C. G. *et al.* Broad and potent activity against SARS-like viruses by an engineered
744 human monoclonal antibody. *Science* **371**, 823–829 (2021).

745 56. Sette, A. & Crotty, S. Adaptive immunity to SARS-CoV-2 and COVID-19. *Cell* **184**, 861–
746 880 (2021).

747 57. Stettler, K. *et al.* Specificity, cross-reactivity and function of antibodies elicited by Zika virus
748 infection. *Science* **353**, aaf8505 (2016).

749

750 **FIGURE LEGENDS**

751 **Figure 1.** VIR-7831 and VIR-7831 bind S and neutralize SARS-CoV-2 virus and S variants of concern in
752 vitro. a) Binding of VIR-7831 (black circles) and VIR-7832 (blue squares) to SARS-CoV-2 RBD was
753 tested by ELISA. Shown is the average of four replicates and SD derived from three independent
754 experiments. b) Association and dissociation profiles of VIR-7831 to SARS-CoV-2-RBD were measured
755 using SPR. The double reference subtracted curves (shown for single replicates) are plotted together with
756 the curve fit in black (obscured by close overlay with the data). Values are from two independent
757 experiments. c) Binding of VIR-7831 (black circles) and VIR-7832 (blue squares) to cell-surface S
758 protein was determined by flow cytometry. Data are expressed as the percentage of the positive cells.
759 Results shown are from one experiment and representative of three independent experiments performed.
760 d) In vitro neutralization of live SARS-CoV-2 by different concentrations of VIR-7831 (left) and VIR-
761 7832 (right) measured by nucleocapsid staining 6-hours post-infection. Results shown are from one
762 experiment and representative of at least three independent experiments performed.

763 **Figure 2.** VIR-7831 and VIR-7832 demonstrate effector function in vitro. In vitro effector function (a-e)
764 activation profiles of human FcγRIIa (a), FcγRIIb (b), FcγRIIIa low-affinity (F158) (c) or FcγRIIIa high-
765 affinity binding allele (V158) (d) using bioreporter assays using S-expressing CHO cells as the target

766 antigen. Data points show means± SD of duplicates. NK-cell mediated killing (ADCC) of S-expressing
767 CHO cells using freshly isolated cells from two donors previously genotyped for homozygous expression
768 of low-affinity (F/F158) (e) or high-affinity (V/V158) FcγRIIIa (f). Data points are means of
769 quadruplicates ± SD. g) Antibody-dependent cellular phagocytosis (ADCP) using S-expressing CHO cells
770 and freshly isolated PBMCs. Data represent the means of duplicates ± SD.

771 **Figure 3.** VIR-7831 shows in vivo efficacy in a hamster SARS-CoV-2 model of infection. a) Overview
772 of hamster in vivo study design. b) and c) Animal weight over time as a percent of starting weight in
773 animals dosed a Day -1 (b) or Day -2 (c). Medians of at least N=6 animals and interquartile range are
774 shown. d) and e) Day 4 terminal weights expressed as a percentage of starting weight for animals dosed at
775 Day -1 (d) or Day -2 (e). Bar denotes median values. f) and g) Day 4 lung viral load in Day -1 (f) or Day -
776 2 (g) treated animals as assessed by RT-qPCR. Bar denotes median values. h) and i) infectious virus in
777 lung at Day 4 for Day -1 (h) or Day -2 (i) dosed animals. Bar denotes median values. ns=not significant,
778 ** = $p<0.05$, and *** = <0.005 as assessed by the Mann-Whitney U-test.

779 **Table 1.** VIR-7831 and VIR-7832 retain activity against S variants of concern in an authentic virus
780 system**.** Average fold change in VIR-7831 and VIR-7832 IC_{50} compared to relative wild-type controls for
781 S variants tested in an authentic virus system. Data shown are averages of at least two independent
782 experiments.

783 **Table 2.** VIR-7831 and VIR-7832 retain activity against S variants of concern in a pseudotyped virus
784 system**.** Average fold change in VIR-7831 and VIR-7832 IC_{50} compared to relative wild-type controls for
785 S variants tested in a VSV/VeroE6 pseudotyped virus system. Data shown are averages of at least two
786 independent experiments.

787 **Table 3.** VIR-7831 and VIR-7832 retain activity against variants that confer resistance to authorized
788 mAbs. Activity of VIR-7831 against variants conferring reduced susceptibility to bamlanivimab,
789 imdevimab or casirivimab in a VSV/VeroE6 pseudotyped virus system. The geometric mean of IC_{50}s and

790 average fold-change versus the relative wild-type control from at least two independent experiments are
791 shown.

792 **Table 4.** The VIR-7831/VIR-7832 epitope is highly conserved. Conservation data comprising >1,000,000
793 sequences from the GISAID database and variants at each position are shown. Variants in bold were
794 tested in a pseudotyped virus assay.

795 **Table 5.** Activity of VIR-7831 against epitope variants. VIR-7831/VIR-7832 epitope variants detected in
796 sequences from the GISAID database were tested in a VSV/VeroE6 pseudotyped virus system. The
797 geometric mean of IC_{50}s and average fold-change versus the relative wild-type control from at least two
798 independent experiments are shown. Variants marked with "a" indicates that the data shown are from the
799 parental antibody S309.

800 **Supplemental Figure 1.** Binding of VIR-7831 and VIR-7832 to human FcγRs and C1q as measured by
801 SPR. Binding of VIR-7831 and VIR-7832 to a) human FcγRIIa (H131 and R131 alleles), FcγRIIIa (F158
802 and V158 alleles) and FcγRIIb were measured using SPR. Biotinylated purified FcγRs were captured on
803 the sensor chip surface prior to injection of VIR-7831 or VIR-7832. Association and dissociation profiles
804 (separated by the vertical dotted line) were measured in real time as change in the SPR signal. b) Binding
805 of VIR-7831 and VIR-7832 to complement component C1q was measured using BLI on an Octet Red96
806 instrument. Association and dissociation profiles (separated by the vertical dotted line) were measured in
807 real time as change in the interference pattern.

808 **Supplemental Figure 2.** Sub-neutralizing concentrations of VIR-7831 and VIR-7832 do not enhance
809 viral entry, viral replication or cytokine production in vitro. Internalization (a) and replication (b) of
810 SARS-CoV-2 was evaluated in VeroE6, moDCs or PBMCs at various timepoints. Two independent
811 experiments with human moDCs and PBMCs from three individual donors were analyzed (5 unique
812 moDC donors, 6 unique PBMC donors total between two experiments). VeroE6 cells were run in
813 duplicate for both independent experiments. Data from each replicate well from two independent

814 experiments are plotted as individual points, with horizontal lines representing the median. Mann-
815 Whitney U-test comparison to no antibody group, *$p<0.05$. c) Supernatant cytokine and chemokine levels
816 as measured by MSD at the indicated time post infection. Data from two independent experiments (three
817 replicates each, five unique donors) are plotted as the mean and SD.

818 **Supplemental Figure 3.** Overview of VIR-7832 resistance selection method. All passaging was
819 conducted in duplicate wells. (a) VIR-7832 concentration was increased during each passage. P3 X
820 indicates passage 3 virus, after which virus was lost with subsequent increases in concentration. In (b) and
821 (c), p3X denotes where passage 3 virus from (a) was used to initiate (b) viral lineage 1 and (c) viral
822 lineage 2. Arrows indicate passages that were subjected to sequence analysis, and * indicate the passages
823 in lineage 1 with no detectable virus or CPE. Selection continued for a total of eight passages.

824 **Supplemental Table 1.** Amino acid substitutions identified in the SARS-CoV-2 S upon in vitro selection
825 with VIR-7832. Spike gene sequences were compared to a SARS-CoV-2 reference sequence (NCBI:
826 NC_045512.2) to identify variants. Fold-changes in IC_{50} were determined compared to the SARS-CoV-2
827 virus stock.

828 **Supplemental Table 2.** VIR-7831 and VIR-7832 activity against selected S variants. VIR-7831/VIR-
829 7832 epitope variants observed by in vitro resistance selection were individually tested in a VSV/VeroE6
830 pseudotyped virus system. The geometric mean of IC_{50}s and average fold-change versus the relative wild-
831 type control from at least two independent experiments are shown.

832

Figure 1

a)

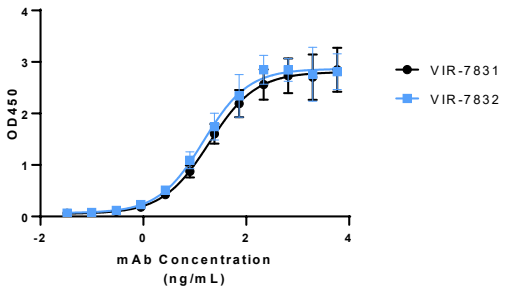

b)

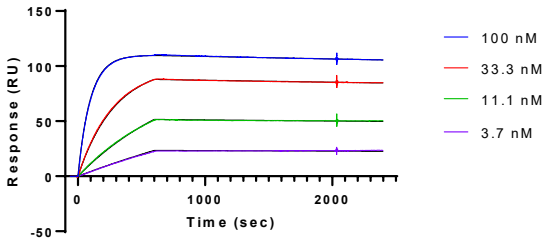

c)

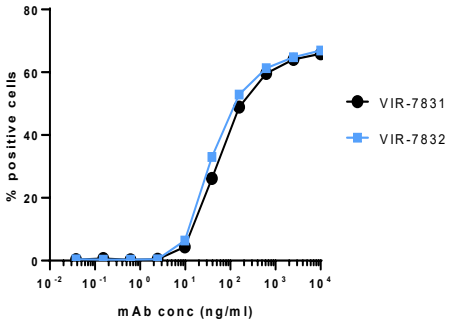

d)

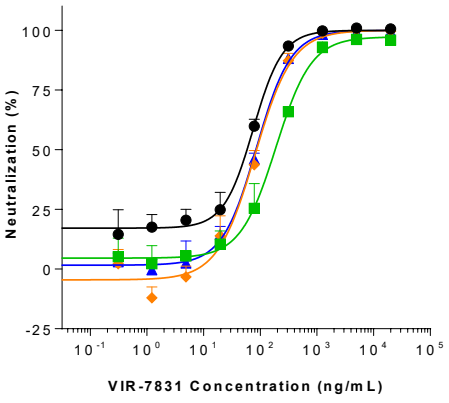

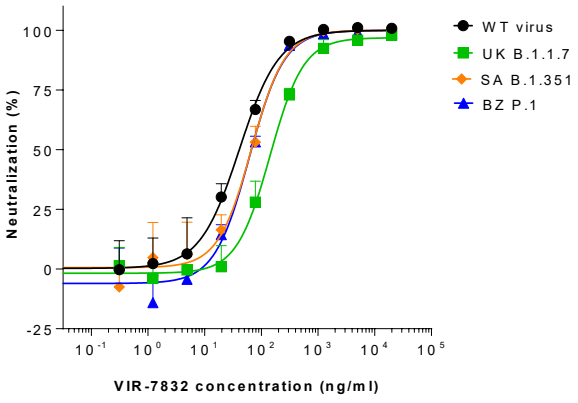

Figure 2

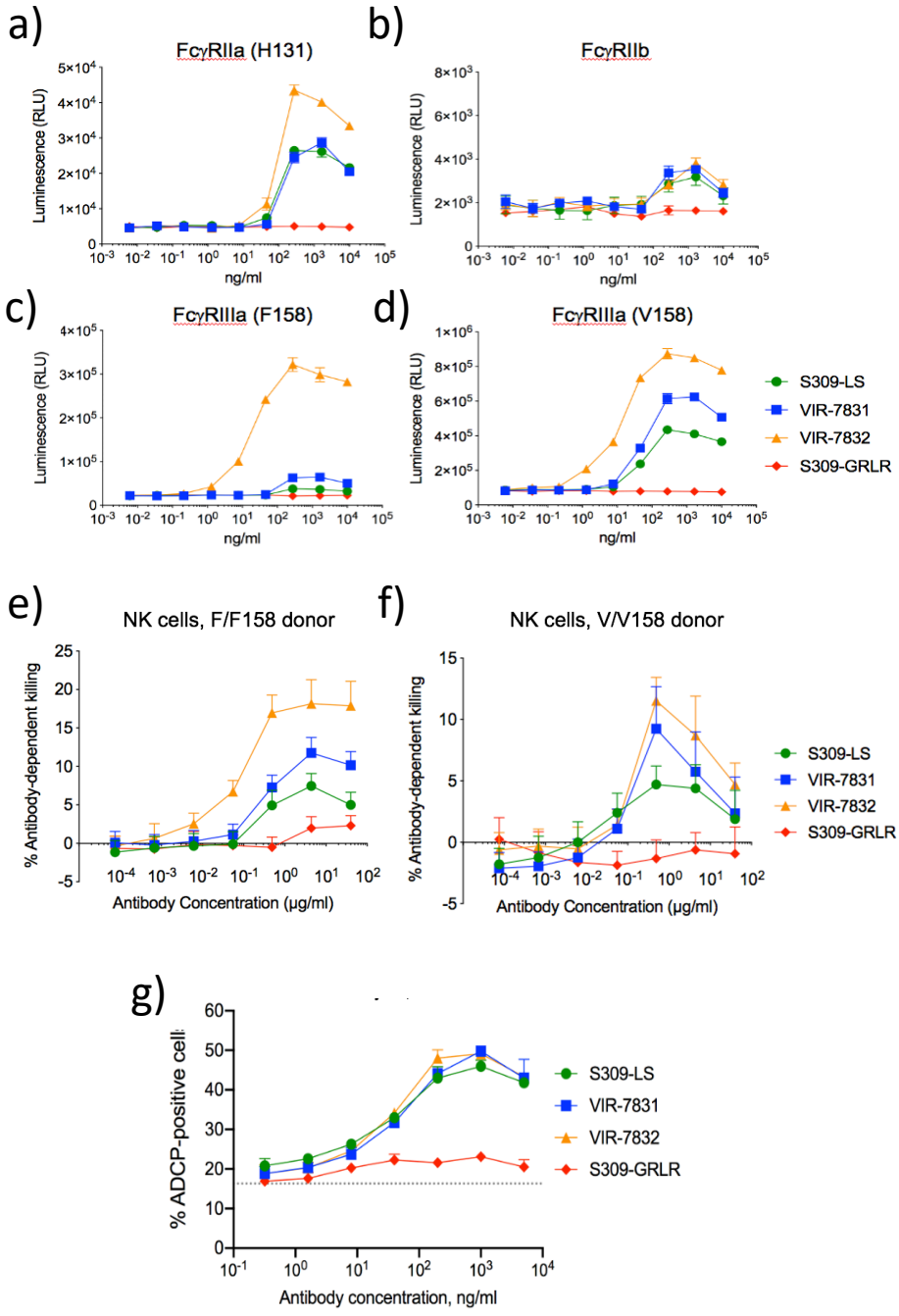
a)
FcγRIIa (H131)
Luminescence (RLU)
ng/ml
b)
FcγRIIb
Luminescence (RLU)
ng/ml
c)
FcγRIIIa (F158)
Luminescence (RLU)
ng/ml
d)
FcγRIIIa (V158)
Luminescence (RLU)
ng/ml
S309-LS
VIR-7831
VIR-7832
S309-GRLR
e)
NK cells, F/F158 donor
% Antibody-dependent killing
Antibody Concentration (μg/ml)
f)
NK cells, V/V158 donor
% Antibody-dependent killing
Antibody Concentration (μg/ml)
S309-LS
VIR-7831
VIR-7832
S309-GRLR
g)
% ADCP-positive cell
Antibody concentration, ng/ml
S309-LS
VIR-7831
VIR-7832
S309-GRLR

Figure 3

a)

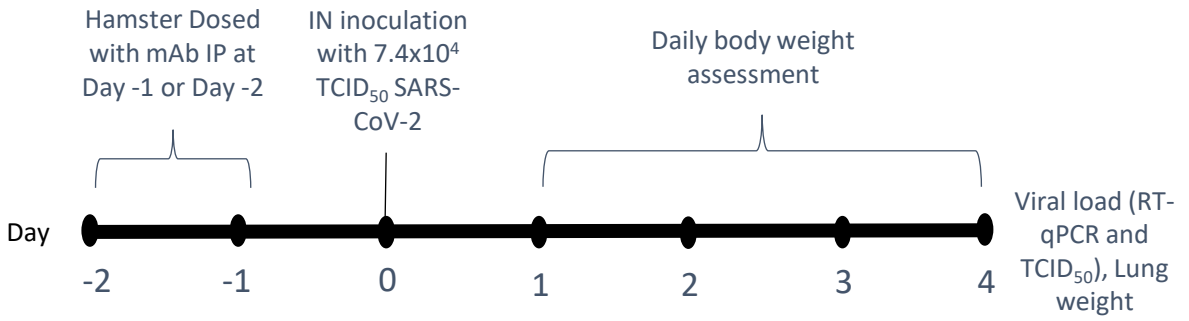

b)

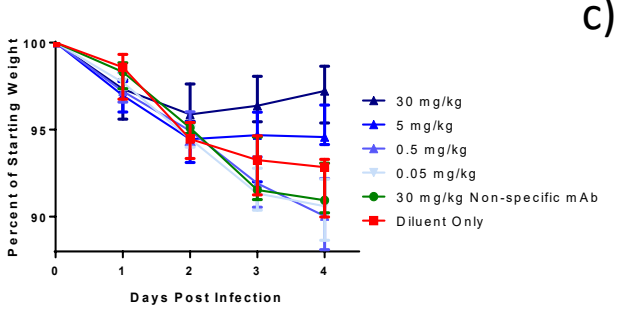

c)

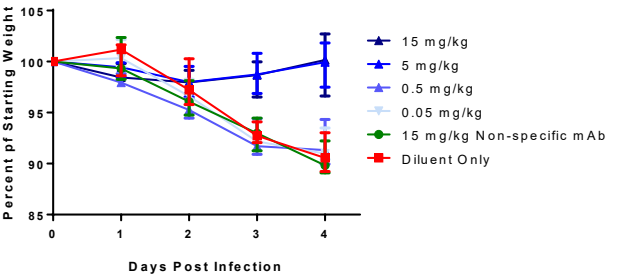

d)

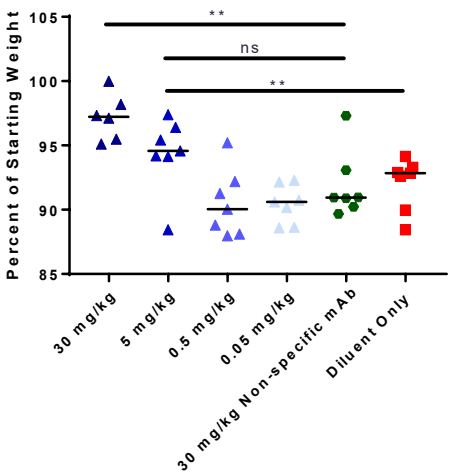

e)

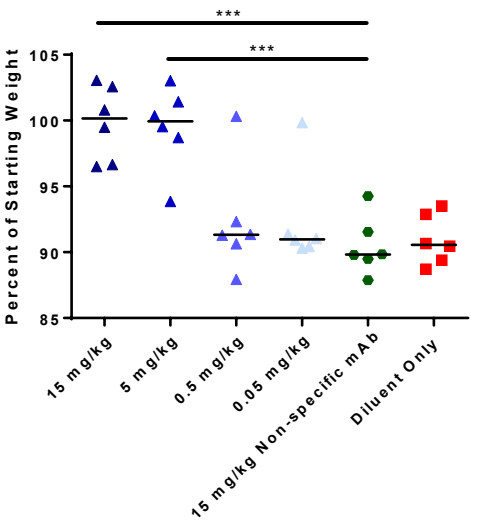

f)

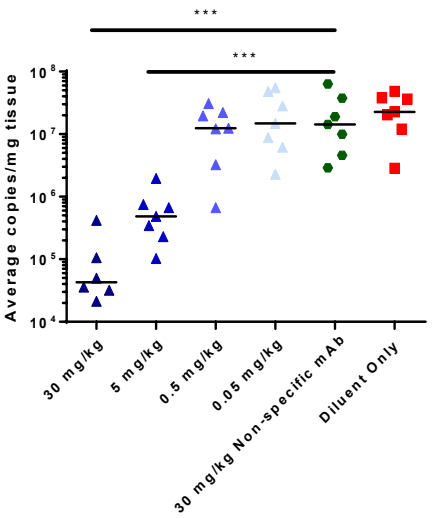

g)

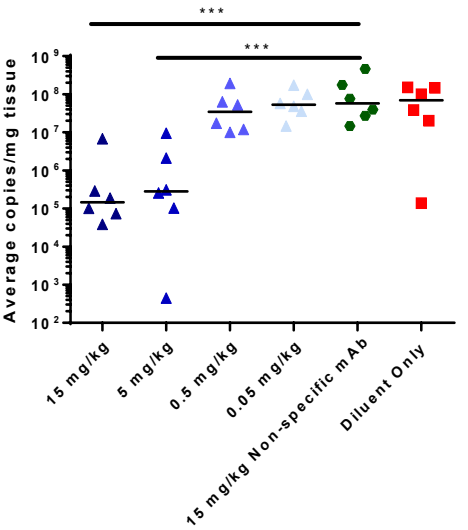

h)

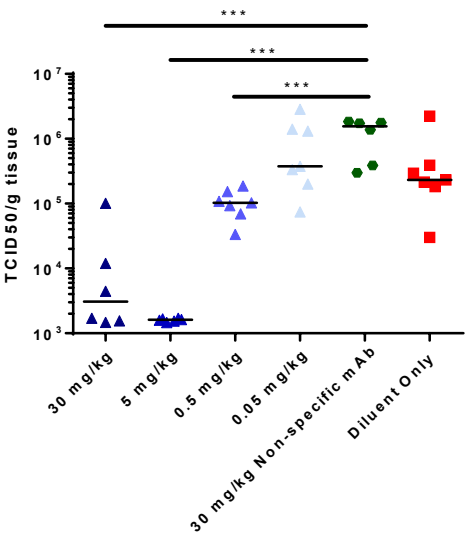

i)

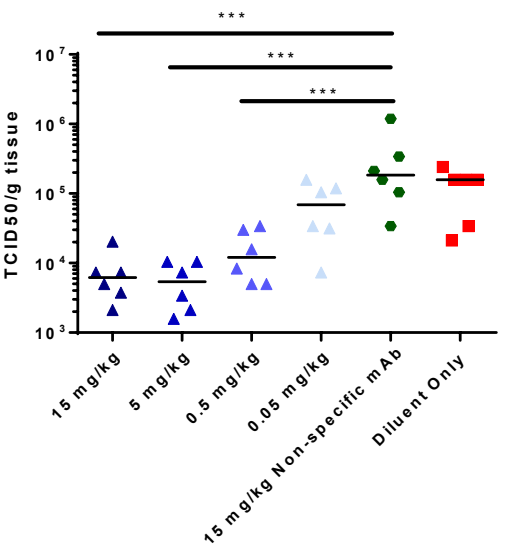

Table 1

SARS-CoV-2 Variant	**Geometric Mean VIR-7831 IC_{50} (ng/ml) (Average Fold Change IC_{50} vs. Wild-Type)**	**Geometric Mean VIR-7831 IC_{90} (ng/ml) (Average Fold Change IC_{90} vs. Wild-Type)**	**Geometric Mean VIR-7832 IC_{50} (ng/ml) (Average Fold Change IC_{50} vs. Wild-Type)**	**Geometric Mean VIR-7832 IC_{90} (ng/ml) (Average Fold Change IC_{90} vs. Wild-Type)**
UK (B.1.1.7)	187.15 (3.0)	1246.86 (4.1)	181.12 (3.1)	1222.95 (3.7)
South Africa (B.1.351)	71.89 (1.2)	385.01 (1.3)	59.67 (1.1)	309.84 (0.9)
Brazil (P.1)	73.11 (1.6)	335.79 (1.4)	48.94 (1.2)	217.02 (0.9)

Table 2

Variant	**Spike Mutations**	**Fold-Change in VIR-7831 IC_{50} vs. Wild-type**	**Fold-Change in VIR-7832 IC_{50} vs. Wild-type**
South Africa (B.1.351)	L18F, D80A, D215G, R246I, K417N, E484K, N501Y, D614G, A701V	0.6	0.7
UK (B.1.1.7)	H69-, V70-, Y144-, N501Y, A570D, D614G, P681H, T716I, S982A, D1118H	2.3	2.5
Brazil (P.1)	D138Y, D614G, E484K, H655Y, K417T, L18F, N501Y, P26S, R190S, T1027I, T20N, V1176F	0.4	0.4
Mexico/Swiss (B.1.1.519)	T478K, D614G, P681H, T732A	0.8	NT
New York (B.1.526)	L5F, T95I, D253G, E484K, D614G, A701V	0.6	NT
Scotland (B.1.258)	H69-, V70-, N439K, D614G,	0.9	NT
Nigeria (B.1.525)	Q52R, A67V, H69-, V70-, Y144-, E484K, D614G, Q677H, F888L	0.9	NT
US (R.2)	E484K, D614G, Q677H, T732S, E1202Q	0.8	NT
California (B.1.427/B.1.429)	S13I, W152C, L452R, D614G	0.9	NT
Liverpool (A.23.1)	R102I, F157L, V367F, E484K, Q613H, P681R	1.1	NT

Table 3

Amino Acid position	Substitution / Deletion	mAb with Reduced Susceptibility	Variants in Tested Spike Sequence	VIR-7831 EC_{50} (ng/ml)	Average Fold Change in EC_{50} Compared to Relative Wild-Type
E406	W	casirivimab+ imdevimab	E406W	53.66	0.74
K417	E	casirivimab	K417E	67.71	0.89
N439	K	imdevimab	N439K, D614G	17.05	0.86
N440	D	imdevimab	N440D	80.47	1.29
N440	K	imdevimab	N440K, D614G	19.99	0.48
K444	Q	imdevimab	K444Q	79.68	1.11
V445	A	imdevimab	V445A	41.74	3.38
G446	V/I	imdevimab	G446V, D614G	18.41	1.50
Y453	F	casirivimab	G261D, Y453F	27.28	2.19
L455	F	casirivimab	L455F, D614G	21.65	0.56
G476	S	casirivimab	G476S	36.97	2.94
E484	K	bamlanivimab	E484K, D614G	12.91	0.33
F486	V/I	casirivimab	F486V	82.24	1.10
Y489	H	casirivimab	Y489H	92.29	1.48
F490	S	bamlanivimab	F490S	33.10	0.85
Q493	K	casirivimab, bamlanivimab	Q483K	69.79	0.98
S494	P	casirivimab, bamlanivimab	S494P, D614G	29.10	2.50

Table 4

Amino Acid Position	Reference Amino Acid[a]	Variants Identified in order of Prevalence[b]	Percent Reference AA Conservation
332	I	V, T	>99.99
333	T	**I**, K	>99.99
334	N	**K,** H, Y, D	>99.99
335	L	**F**, S, M	99.99
336	C	S	>99.99
337	P	**S, T, L, H, R**	>99.99
339	G	**D**, **S,** V, **C**, F	99.98
340	E	D, **K, G**, **A,** Q	99.99
341	V	**I**, A, P, S	99.99
343	N	S	>99.99
344	A	**S**, V, **T**, D, F, P	99.98
345	T	**S,** I, N	>99.99
346	R	**K, I, S,** G, **T**, F	99.94
354	N	**D, K, S**, **H**, G, Y	99.96
356	K	**R,** M, **N**, T, E, Y, G	99.99
357	R	**K, I** , G	99.95
358	I	**V**, T, **L**, A, E, F	>99.99
359	S	**N**, T, **R**, **G**, I	99.99
360	N	S, A, T, Y	>99.99
361	C	T	>99.99
440	N	**K**, T, **Y**, **S**, **D**, I, H	99.89
441	L	**F**, **I**, R, V	>99.99
509	R	I, K, S, T, P	>99.99

Table 5

Epitope Reference Amino Acid	Amino Acid Changes in Spike protein	Geomean Neutralization EC_{50} (ng/mL)	Average Fold-Change VIR-7831 EC_{50} Relative to Wild-Type
T333	T333I, D614G	30.93	0.59
N334	N334K, D614G	45.36	1.27
L335	L335F	29.19	0.81
P337	P337H, D614G[a]	225.49	7.50
	P337L, D614G[a]	5241.44	180.46
	P337R, D614G[a]	>10000	>276
	P337S, D614G	127.69	1.26
	P337T, D614G[a]	199.78	5.38
G339	G339D, D614G	117.38	1.18
	G339S, D614G	32.67	0.63
	G339C, D614G	68.79	1.18
E340	E340A	>10000	>100
	E340K	>10000	>297
	E340G, D614G[a]	1013.97	27.47
V341	V341I, D614G	14.6	0.16
A344	A344S	92.19	0.89
	A344T, D614G	40.94	0.62
R346	R346K, D614G	24.76	0.72
	R346I, D614G	65.39	1.25
	R346S, D614G	42.87	0.82
	R346T, D614G	89.04	1.25
N354	N354D	104.8	1.00
	N354K, T95I	70.62	0.76
	N354S, D614G	61.78	0.89
	N354H, D614G	74.88	1.06
K356	K356R, D614G	29.61	0.57
	K356N, D614G	53.22	1.12
R357	R357K, D614G	39.13	0.75
	R357I, D614G	46.41	0.98
I358	I358V, D614G	32.71	0.70
	I358L	44.01	0.80
S359	S359N	95.55	0.96
	S359G, D614G	37.56	0.80
	S359R, D614G	62.0	0.89
N440	N440K, D614G	19.99	0.48
	N440Y, D614G	42.65	0.68
	N440S, D614G	51.34	0.73
L441	L441F, D614G	25.21	0.40
	L441I, D614G	32.96	0.70

Supplemental Figure 1

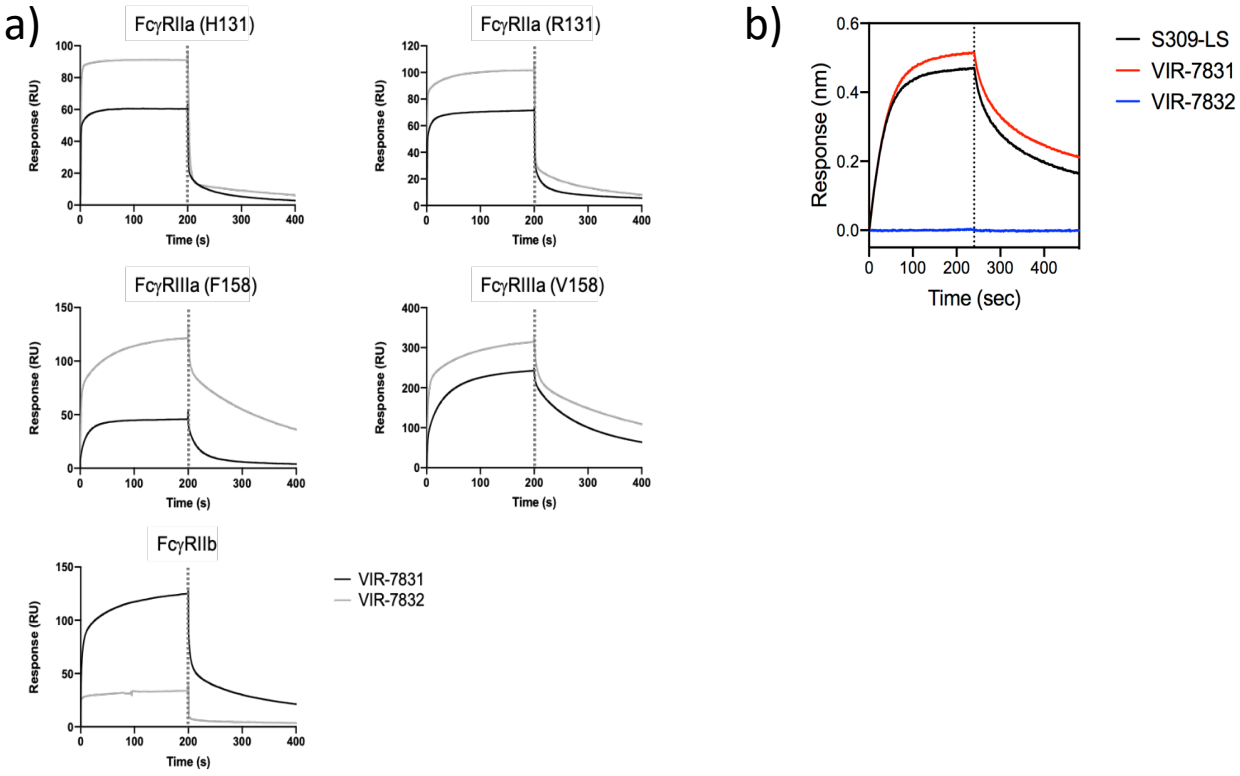

Supplemental Figure 2

a)

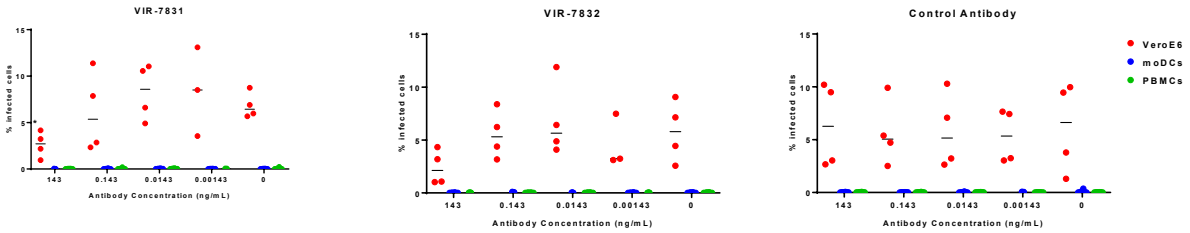

b)

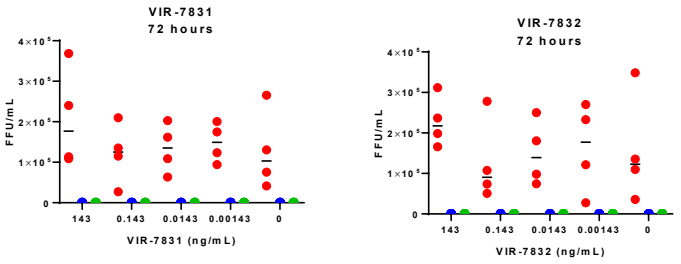

c)

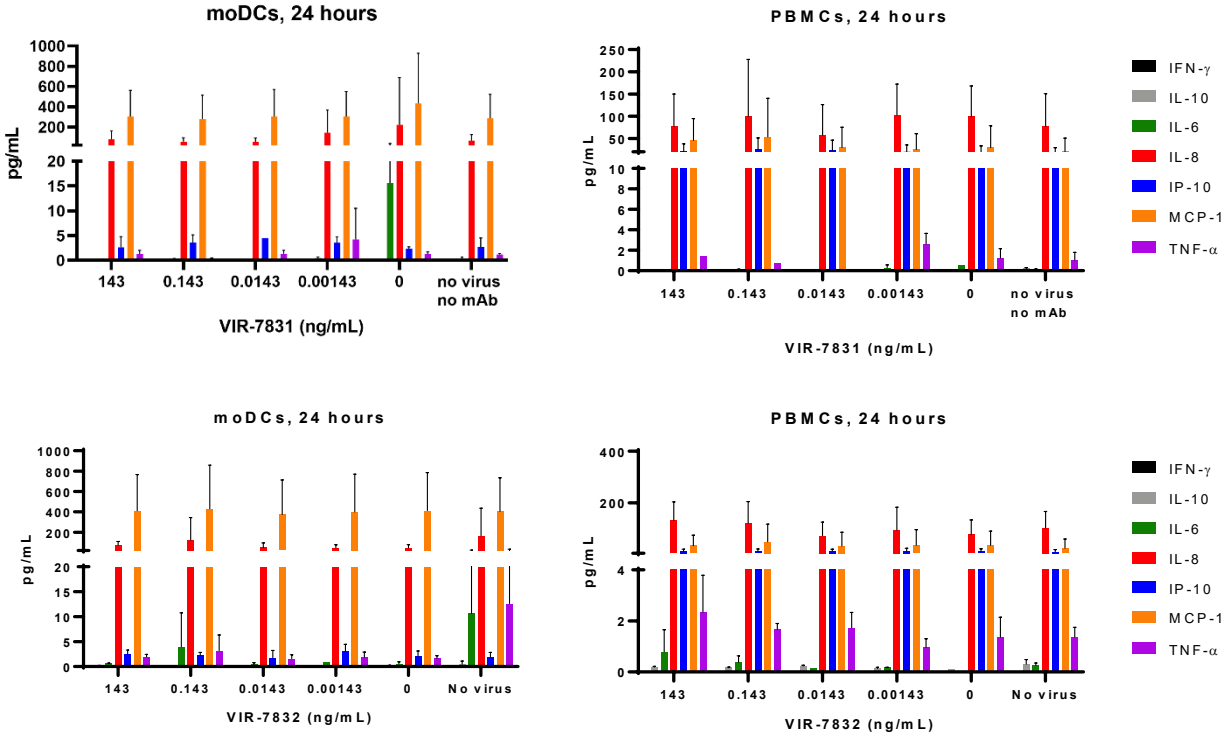

Supplemental Figure 3

a)

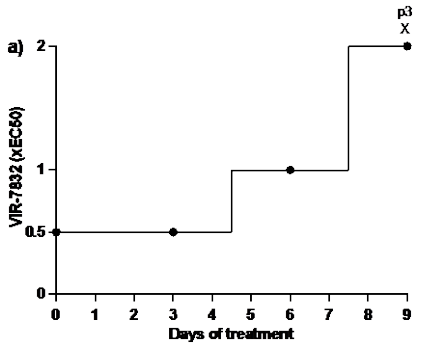

b)

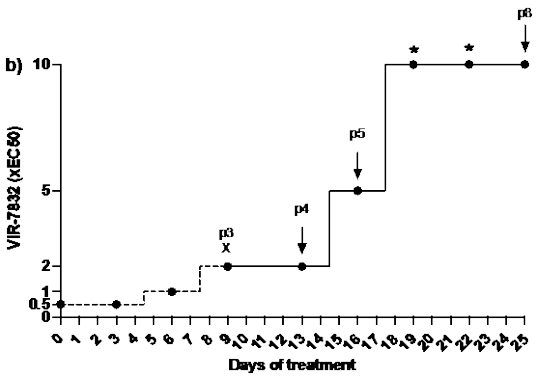

c)

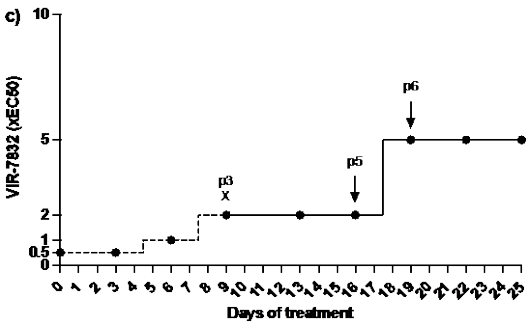

Supplemental Table 1

Passage	**Spike Gene Amino Acid Substitution (Freq)** [a,b]	**EC_{50} (µg/mL)**	**Fold Change in EC_{50} to WT**[c]
SARS-CoV-2 virus stock[c]	H66R (5.7%) N74K (12.6%) T76I (5.6%) 215-216insKLRS (60.9%) H655Y (3.1%)	0.06	NA
VIR-7832 Lineage 1, passage 4	215-216insKLRS (74.5%) 675-679 del (20.6%)	0.34	5.64
VIR-7832 Lineage 1, passage 5	215-216insKLRS (74.6%) 675-679del (66.0%)	0.35	5.93
VIR-7832 Lineage 1, passage 8	215-216insKLRS (74.7%) E340A (98.7%) 675-679del (84.5%)	ND	>10
VIR-7832 Lineage 2, passage 5	215-216insKLRS (73.9%) 675-679del (47.3%) R682W (4.9%) V1128F (3.5%)	0.32	5.40
VIR-7832 Lineage 2, passage 6	215-216insKLRS (75.3%) 675-679del (74.2%) R682W (4.9%) V1128F (30.9%)	0.39	6.54

Supplemental Table 2

Amino Acid Changes in Spike protein	VIR-7831		VIR-7832	
	Geomean Neutralization EC_{50} (ng/mL)	Fold Change Relative to Wild-Type	Geomean Neutralization EC_{50} (ng/mL)	Fold Change Relative to Wild-Type
Wild Type[a]	104.46	NA	100.75	NA
E340A	> 10,000	>100	> 10,000	> 107
R682W	53.96	0.52	47.78	0.49
V1128F	50.65	0.53	49.69	0.60